medRxiv preprint doi: https://doi.org/10.1101/2020.09.22.20199174; this version posted September 23, 2020. The copyright holder for this preprint (which was not certified by peer review) is the author/funder, who has granted medRxiv a license to display the preprint in perpetuity.

It is made available under a CC-BY-ND 4.0 International license .

Optimal Dynamic Prioritization of Scarce COVID-19 Vaccines

Authors:

Jack H. Buckner,[1*] Gerardo Chowell,[2] Michael R. Springborn[3*]

Affiliations:

[1]Graduate Group in Ecology, University of California Davis, One Shields Ave, Davis, CA

[2]Department of Population Health Sciences, School of Public Health, Georgia State University, Atlanta, GA

[3]Department of Environmental Science and Policy, University of California, Davis, One Shields Ave, Davis, CA

*To whom correspondence should be addressed: jhbuckner@ucdavis.edu and mspringborn@ucdavis.edu

September 22, 2020

Abstract. Multiple promising COVID-19 vaccines are under rapid development, with deployment of the initial supply expected by 2021. Careful design of a vaccine prioritization strategy across socio-demographic groups is an imminent and crucial public policy challenge given that (1) the eventual vaccine supply will be highly constrained for at least the first several months of the vaccination campaign, and (2) there are stark differences in transmission and severity of impacts from SARS-CoV-2 across groups. Previous experience with vaccine development mid-pandemic offers limited insights for SARS-CoV-2 prioritization: SARS and Zika vaccine development was incomplete when those outbreaks ended and the epidemiology of endemic human influenza viruses differ substantially from that of SARS-CoV-2. We assess the optimal allocation of a limited and dynamic COVID-19 vaccine supply in the U.S. across socio-demographic groups differentiated by age and essential worker status. The transmission dynamics are modeled using a compartmental (SEIR) model parameterized to capture our current understanding of the transmission and epidemiological characteristics of COVID-19, including key sources of group heterogeneity (susceptibility, severity, and contact rates). We investigate tradeoffs between three alternative policy objectives: minimizing infections, years of life lost, or deaths. Moreover, we model dynamic vaccine prioritization policies that respond to changes in the epidemiological status of the population as SARS-CoV-2 continues its march. Because contacts tend to be concentrated within age groups, there is diminishing marginal returns as vaccination coverage increases in a given group, increasing the group's protective immunity against infection and mortality. We find that optimal prioritization consistently targets older essential workers. However, depending on the policy objective, younger essential workers are prioritized to minimize infections or seniors in order to minimize mortality. Optimal prioritization outperforms non-targeted vaccination strategies by up to 18% depending on the outcome optimized. For example, in our baseline model, cumulative mortality decreased on average by 17% (25,000 deaths in the U.S. population) over the course of the outbreak.

NOTE: This preprint reports new research that has not been certified by peer review and should not be used to guide clinical practice.

medRxiv preprint doi: https://doi.org/10.1101/2020.09.22.20199174; this version posted September 23, 2020. The copyright holder for this preprint (which was not certified by peer review) is the author/funder, who has granted medRxiv a license to display the preprint in perpetuity.

It is made available under a CC-BY-ND 4.0 International license .

1 Introduction

As the novel coronavirus (SARS-CoV-2) continues to spread in many countries despite intervention efforts, public health experts see a vaccine as essential to dramatically reduce mortality burden and possibly halt local transmission in the short term (Corey et al., 2020). Novel coronavirus disease 2019 (COVID-19) has resulted in over 930,000 confirmed deaths globally (Dong et al., 2020) as of mid-September 2020. Multiple promising vaccines are under rapid development, with deployment possible in late 2020 or early 2021 (USHSS 2020). While the vaccine supply schedule remains highly uncertain, it is clear that vaccine availability will be highly constrained for at least several months after launching the vaccination campaign (Emanuel et al., 2020). This scarcity, combined with stark differences in the spread and impact of SARS-CoV-2 across demographic groups, means that prioritization of the vaccine is an imminent and crucial public health challenge, and as such under active discussion by the "Advisory Committee on Immunization Practices (ACIP) of the US Centers for Disease Control and Prevention (CDC) and the National Academy of Medicine (NAM), as well as globally at the World Health Organization (WHO) and elsewhere" (Toner et al., 2020).

An effective public health policy for pandemic vaccine allocation requires an understanding of transmission and epidemiological characteristics of the novel disease across different socio-demographic groups, knowledge of the mechanisms that drive the spread of virus in the population as well as reliable estimates of prevalence and built-up immunity levels about the time immunization strategies are set to begin. These key components are then integrated into a mathematical and statistical modeling framework of the transmission dynamics of the novel pathogen. Such an analytic framework can then be utilized to investigate the optimal vaccine allocation strategies to achieve a defined public health objective while taking into account uncertainties surrounding the vaccine efficacy and temporal changes in vaccine availability (Medlock and Galvani, 2009; Chowell et al., 2009).

Previous experience with vaccine development mid-pandemic offers limited insights for SARS-CoV-2 prioritization. SARS and Zika vaccine development was incomplete when those outbreaks ended (Lurie et al., 2020). In 2009, as the novel A/H1N1 influenza virus continued to spread across the United States, researchers investigated optimal vaccination strategies using an age-structured dynamical model. They found that school-aged children and their parents should be prioritized, a strategy that would indirectly protect individuals at higher risk of severe health outcomes (Medlock and Galvani, 2009). Sharp differences in the epidemiology of human influenza and COVID-19 indicate that vaccination strategies against the ongoing pandemic should not simply mirror vaccination policies against influenza. For example, COVID 19 is associated with lower susceptibility to infection among children and adolescents (Davies et al., 2020) and has a substantially higher infection fatality rate that increases markedly with age (Verity et al., 2020). Toner et al. (2020, p. 24) provide a detailed overview of the 2018 pandemic influenza vaccination plan and conclude that, "the priority scheme envisioned...does not comport with the realities of the COVID-19 pandemic and new guidance is needed."

We develop and apply an analytic framework to assess the optimal and gradual allocation of limited COVID-19 vaccine supply in the U.S. across socio-demographic groups differentiated by age and essential worker status.

medRxiv preprint doi: https://doi.org/10.1101/2020.09.22.20199174; this version posted September 23, 2020. The copyright holder for this preprint (which was not certified by peer review) is the author/funder, who has granted medRxiv a license to display the preprint in perpetuity.

It is made available under a CC-BY-ND 4.0 International license .

Toner et al. (2020) emphasize the importance of considering the prioritization of essential workers "who have been overlooked in previous allocation schemes". The transmission dynamics are modeled using a compartmental model parameterized to capture our current understanding of the epidemiology of COVID-19. We investigate three alternative policy objectives: minimizing expected cases, years of life lost, or deaths. Moreover, we consider dynamic vaccine prioritization policies that respond to changes in the epidemiological status of the population as the novel coronavirus continues its march (shares of the population in different disease states). We construct educated guesses of initial population conditions when a vaccine first arrives (e.g., in late 2020 or the first half of 2021) by assessing current conditions and projections of disease burden (as of September 2020). A central constraint is the expected scarcity of the ongoing supply of vaccines (e.g., sufficient to vaccinate 60% of the population in the first 6 months). We focus on the challenge of allocating vaccines across the general population, specifically the distribution of vaccine remaining after specialized top priority groups like medical personnel and front line workers are covered.

To our knowledge there are no published analyses of optimal COVID-19 vaccination prioritization. Analysis in preprint form is limited to Matrajt et al. (2020) and Bubar et al. (2020). Both consider the optimal allocation of vaccines across five or more age groups. Their approaches feature rich exploration of policy sensitivity to vaccine efficacy and availability. Matrajt et al. (2020) is particularly detailed in this respect, while Bubar et al. (2020) extend to consider differences in demographics and contact rates across multiple countries. In our analysis we take a deeper approach to the behavioral, demographic and decision models by addressing social distancing, essential worker groups, and allocation polices that can change over time. Finally, Gallagher et al. (2020) use simulation without optimization to explore implications of vaccines with various levels of direct and indirect protection.

To date, general ethical guiding frameworks for guiding vaccine prioritization decision making have received more attention. Toner et al. (2020) emphasize promoting three ethical values: the common good; fairness and equity; and legitimacy, trust and communal contributions to decision-making. Emanuel et al. (2020) promote four ethical values: maximizing benefits, treating equally, instrumental value, and priority to the worst off. Our analytic focus on minimizing new infections, years of life lost, or deaths emerges from promoting "the common good" or "maximizing benefits". Issues of fairness and equity and protecting the worst off are not directly analyzed here but remain critical considerations.

A number of key model components are still highly uncertain in advance of the vaccine's arrival, including: initial epidemiological conditions in the population, degree of vaccine scarcity, vaccine efficacy and level of social distancing in effect as the vaccine is allocated (Toner et al., 2020). There also does not exist a unique preferred structure for socio-demographic groups or a singular consensus objective. Thus, we consider a number of alternative objectives and scenarios based on plausible specifications of the model. In our results we highlight findings that are either (1) consistent across the scenarios, (2) depend on uncertainties that can be narrowed down when a vaccine arrives [e.g., the initial disease prevalence], or (3) a matter of subjective choice [e.g., the objective].

For the sake of simplicity, we do not address in the model an important set of additional complex feedback processes between health status and opening of schools, workplaces and other institutions. While we limit policy objectives to

medRxiv preprint doi: https://doi.org/10.1101/2020.09.22.20199174; this version posted September 23, 2020. The copyright holder for this preprint (which was not certified by peer review) is the author/funder, who has granted medRxiv a license to display the preprint in perpetuity.

It is made available under a CC-BY-ND 4.0 International license .

a concise metric of health outcomes (minimizing expected cases, years of life lost, or deaths) we acknowledge that other values of returning to school, work and social life are important. Finally, we do not address additional vaccine complications, such as temporary efficacy, potential side effects or any failure to take a second dose of the vaccine if necessary.

Given these assumptions we find that optimal allocation strategies are responsive to both the initial and evolving epidemiological landscape of the disease. When deaths are considered, vaccines are initially allocated to older essential workers $40-59$ yrs. followed by seniors 60+ yrs., when years of life lost are minimized both ages groups of essential workers are prioritized follow by seniors $60-74$ yrs., and when infections are minimized essential workers are prioritized followed by school age children. In general, we find that these results are robust across a range of possible scenarios and parameters sets. However, they are sensitive to changes in vaccine efficacy and susceptibility between age groups, indicating that these will be key uncertainties prior to the vaccines arrival. We found that the optimal strategies outperformed a non-targeted strategy (e.g., distributed proportional to the size of each group) by 8 to 20% for a given target policy objective. For example, in our baseline model incorporating essential worker groups, cumulative pandemic deaths decreased on average by 17% or 25,000 COVID-19 deaths (when applied to the U.S. population) over the course of the outbreak.

2 Model

To investigate the impact of vaccination strategies on the COVID-19 pandemic in the USA, we employed a structured compartmental transmission model similar to Abrams et al. (2020). We incorporated the demographic structure of the population by tracking six age groups in the set $J = \{\text{0-4}, \text{5-19}, \text{20-39}, \text{40-59}, \text{60-74}, \text{75+}\}$. We then extend this set to differentiate essential workers by splitting the two prime working age groups into two groups—nonessential workers (20-39, 40-59) and essential workers (20-39*, 40-59*)—yielding four groups of prime working age individuals and a total of eight demographic groups in $J = \{\text{0-4}, \text{5-19}, \text{20-39}, \text{20-39}^*, \text{40-59}, \text{40-59}^*, \text{60-74}, \text{75+}\}$.

For each demographic group we tracked 9 epidemiological states: susceptible (S), protected by a vaccine (P), vaccinated but unprotected (F), exposed (E), pre-symptomatic (I_{pre}), symptomatic (I_{sym}), asymptomatic (I_{asym}), recovered (R) and deceased (D). In Fig. 1 we display the compartmental diagram describing the transitions between epidemiological states.

We model the COVID-19 transmission dynamics using a system of coupled ordinary differential equations for each demographic group, indexed by i and j. The transmission rate is given by the product of the transmission probability (q), the age-specific susceptibility (s_i), strength of non-pharmaceutical interventions (θ), the relative infectiousness of each symptom type (τ_m)—where $m \in M \equiv \{asym, pre, sym\}$—and the rate of contact ($r_{m,i,j}$) between infected individuals with symptom type m from group j and susceptible individuals from group i. The exogenously given population vaccination rate at time t is given by v, where units of time are days.[1] In our Base model we assume that

[1] In the event that vaccination requires two doses over time, we consider an individual vaccinated upon receipt of the second dose at time t and we assume that v indicates the number of *individuals* that can be vaccinated with the required number of doses.

medRxiv preprint doi: https://doi.org/10.1101/2020.09.22.20199174; this version posted September 23, 2020. The copyright holder for this preprint (which was not certified by peer review) is the author/funder, who has granted medRxiv a license to display the preprint in perpetuity.

It is made available under a CC-BY-ND 4.0 International license .

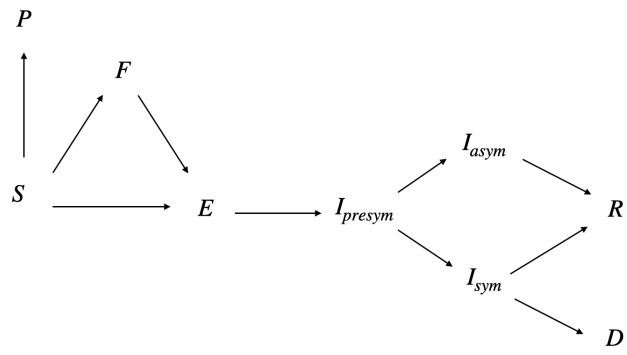

Figure 1: Movement of individuals between disease states.

for each individual the vaccine either works or it does not (though we also consider vaccines that are partially effective for all vaccinated in our sensitivity analysis). Individuals in group i are vaccinated at a rate of $\mu_i v$ and a fraction of the those (ϵ_i) are protected while a fraction remain susceptible and move to the failed vaccination category (F).[2] Once infected, individuals move from exposed to pre-symptomatic at rate D_{exp}^{-1}. Pre-symptomatic individuals become symptomatic or asymptomatic at rates σ_{asym}/D_{pre} and $(1-\sigma_{asym})/D_{pre}$, respectively. Asymptomatic individuals recover at an uniform rate D_{asym}^{-1} and symptomatic individuals either recover or die at a rate of $(1-\delta_a)/D_{sym}$ or δ_a/D_{sym}, respectively, where δ_a is the age-specific infection fatality rate. These assumptions yield the system of differential equations for all groups i in set J:

$$\dot{S}_i = -qs_i\theta\left[\sum_{j\in J}\sum_{m\in M}\tau_m r_{m,i,j} S_i \frac{I_{m,j}}{N_j}\right] - \mu_i v \tag{1}$$

$$\dot{F}_i = -qs_i\theta\left[\sum_{j\in J}\sum_{m\in M}\tau_m r_{m,i,j} F_i \frac{I_{m,j}}{N_j}\right] + (1-\epsilon_i)\mu_i v \tag{2}$$

$$\dot{E}_i = qs_i\theta\left[\sum_{j\in J}\sum_{m\in M}\tau_m r_{m,i,j} (S_i+F_i) \frac{I_{m,j}}{N_j}\right] - E_i/D_{exp} \tag{3}$$

$$\dot{P}_i = \epsilon_i\mu_i v \tag{4}$$

$$\dot{I}_{pre,i} = E_i/D_{exp} - I_{pre,i}/D_{pre} \tag{5}$$

$$\dot{I}_{asym,i} = \sigma_{asym} I_{pre,i}/D_{pre} - I_{asym,i}/D_{asym} \tag{6}$$

$$\dot{I}_{sym,i} = (1-\sigma_{asym}) I_{pre,i}/D_{pre} - I_{sym,i}/D_{sym} \tag{7}$$

$$\dot{R}_i = I_{asym,i}/D_{asym} + (1-\delta_i) I_{sym,i}/D_{sym} \tag{8}$$

$$\dot{D}_i = \delta_i I_{sym,i}/D_{sym}. \tag{9}$$

[2]This vaccine efficacy is inclusive of any efficiency loss from typical handling in the distribution chain.

medRxiv preprint doi: https://doi.org/10.1101/2020.09.22.20199174; this version posted September 23, 2020. The copyright holder for this preprint (which was not certified by peer review) is the author/funder, who has granted medRxiv a license to display the preprint in perpetuity.

It is made available under a CC-BY-ND 4.0 International license .

3 Model parameterization

3.1 Contact rates

Contact rates indicating the level of direct interaction of individuals within and between groups drive the transmission dynamics in the model. We build the contact matrices used in this model from the contact matrices estimated for the United States in Prem et al. (2017). These estimates are given for age groups with five year age increments from 0 to 80 yrs. These estimates were aggregated to provide estimates for the coarser age structure used in our model. We also extend these data to estimate the contact rates of essential workers. A detailed derivation of these contact rates can be found in the appendix A.2, but in short we assume that essential workers have on average the same pattern of contacts as an average worker in the population in the absence of social distancing. We then scale the contact rates for essential and non-essential workers to represent the effects of social distancing and calculate the resulting mixing patterns assuming homogeneity between these groups.

Following, Prem et al. (2017) we construct contact matrices for four classes of locations $x \in \{home, work, school, other\}$. The total contact rate for an asymptomatic individual before the onset of the pandemic is given by the sum of these location specific matrices. However, it is clear that populations are exhibiting social distancing in response to the pandemic (Weill et al., 2020). We further expect symptomatic individuals to change their behavior in response to the illness. We account for these behavioral changes as described below in Section 3.2.

3.2 Social distancing

Expression of symptoms and social distancing policies are likely to change individuals behaviors over time. To model these changes we scaled the contribution of each contact matrix for location/activity x:

$$r_m = \sum_x \alpha_{m,x} * r_x. \tag{10}$$

The weights $\alpha_{m,x}$ depend on disease and symptom status (m) and location/activity (x) as specified in Table 1. We scaled social contacts for symptomatic individuals following changes in behavior observed among symptomatic individuals during the 2009 A/H1N1 pandemic (Van Kerckhove et al., 2013). For those without symptoms (susceptible and asymptomatic) the weights were specified to match reduced levels of social contacts as the product of social distancing policies. Home contact rates were held constant. Since completed research studies to understand changes in work contact rates are not yet available, we select a level based on preliminary survey data across eight U.S. regions collected by the Institute for Transportation Studies at the University of California Davis, which indicates that trips to work have fallen after the onset of the pandemic from an average of 4.1 to 1.9 days, or 54% (Circella, 2020). The work contact rates for both model formulations were set to be consistent with an overall reduction of 54%. This value was used directly in the age-only model and divided into a weight of 100% for essential works and a weight of 9% for nonessential workers in the essential worker model formulation. School contact rates were set to an assumed weight of 30%, to account for a mixed effect of a small fraction of schools remaining open and possible increased

medRxiv preprint doi: https://doi.org/10.1101/2020.09.22.20199174; this version posted September 23, 2020. The copyright holder for this preprint (which was not certified by peer review) is the author/funder, who has granted medRxiv a license to display the preprint in perpetuity.

It is made available under a CC-BY-ND 4.0 International license .

Disease and symptom type	Model	Contact rate weights, $\alpha_{m,x}$			
		home	*work*	*school*	*other*
symptomatic	all	1.0	0.09	0.09	0.25
susceptible,	age-only	1.0	0.54	0.3	0.25
asymptomatic	age and essential workers	1.0	1.0*, 0.09	0.3	0.25

Table 1: Weights on contact rates for a given disease and symptom type (m) and location/activity (x) under social distancing. When essential and non-essential-worker weights are both needed the former is marked with a star.

social contacts between school age children during time that would other wise have been devoted to school. As an alternative scenario, we consider the case of more school contacts with a weight of 70% (see Table 3). Contact in other locations were given an assumed weight of 25%.

The proportion of workers deemed essential, p, was estimated with two components: the total number of workers involved in activities essential to the maintenance of critical services and infrastructure and the fraction of these workers that were required to work in person. The cyber-security and infrastructure security agency of the United States estimates that 70% of the work force is involved in these essential activities (e.g. heath care, telecommunications, information technology systems, defense, food and agriculture, transportation and logistics, energy, water, public works and public safety). We used estimates of the fraction of workers that could successfully complete their duties from home produced by Bartik et al. (2020) who estimated this value at approximately 30%. These two values gave a final proportion of $p = 0.7(1 - 0.3) = 0.49$.

3.3 Transmission rate

The relationship between the basic reproduction number, R_0, and parameters governing transmission and epidemiological characteristics is given by the so-called next-generation matrix:

$$R_0 = max[eigenval\{qD_{pre}\tau_{pre}(r\Delta s)\Delta n + q\sigma_{asym}D_{asym}\tau_{asym}(r\Delta s)\Delta n + q(1-\sigma_{asym})D_{sym}\tau_{sym}(r\Delta s)\Delta n\}], \tag{11}$$

where the maximum eigenvalue operator wraps several terms including r, the social contact matrix, s, the age-specific susceptibility rate, n, a vector of the proportions of the population in each demographic group and Δ, an operator that signifies multiplying each row of a matrix by the corresponding entry in the vector. For symptom type $m \in \{asym, pre, sym\}$, the constants D_m, τ_m and σ_m represent the duration, relative infectiousness of an individual and the probability of type m, respectively.

We first set a baseline $R_0 = 2.5$ as estimated by Kucharski et al. (2020). We then solve for the transmission probability parameter, q, using Equation 11, assuming a naive (pre-pandemic) population. We then scaled q by a fixed factor $\theta \in [0, 1]$ to reflect the impact of non-pharmaceutical interventions (NPI) like masks, hand washing and maintaining distance when contacts are made.

medRxiv preprint doi: https://doi.org/10.1101/2020.09.22.20199174; this version posted September 23, 2020. The copyright holder for this preprint (which was not certified by peer review) is the author/funder, who has granted medRxiv a license to display the preprint in perpetuity.

It is made available under a CC-BY-ND 4.0 International license .

3.4 Initial conditions

Because the expected epidemiological conditions $\{I_{pre}(0), I_{asym}(0), I_{sym}(0), S(0)\}$ by the time the initial vaccine doses are ready for deployment are uncertain, we construct plausible baseline values for the U.S. using estimates of COVID-19 disease burden from the start of the outbreak in February 2020 through present and use projected disease burden estimates by December 1, 2020 taken from near real-time projections by the Institute of Health Metrics and Evaluation (IHME, 2020a). Specifically, we set the initial epidemiological conditions to be consistent with cumulative and current cases by December 1, 2020. These cases are apportioned between demographic groups to reflect the attack rates of COVID-19 for each group under the given social distancing policy.

3.5 Parameter summary for Base case and alternative scenarios

In Table 2 we list and describe the parameters used in the Base model along with the value(s) used and the source (except for contact matrices and social distancing, discussed later). These parameter values reflect moderate restrictions of work and social gatherings and that NPIs other than social distancing (mask wearing, hand washing, spacing between people, etc.) scale the transmission rate q by a factor of $\theta = 0.65$. Consistent with influenza vaccine efficacy, we assume that the COVID-19 vaccine has efficacy of $\epsilon = 0.65$. We assume that there will be a sufficient number of vaccine doses to cover 60% of the population during the first six months of the vaccination campaign—10% per 30 day period—that is available at a constant daily fraction of the population, $v = 0.1/30$. While the Director of the U.S. National Institute of Allergy and Infectious Diseases has indicated that tens of millions of doses are likely to be available in early 2021 (Erman and Mason, 2020), the supply schedule of vaccines is currently unknown.

To address uncertainty in key model model components in advance of the vaccine arrival, we solved for optimal policies for a range of alternative scenarios with different parameters. In Table 3 we summarize the eight alternative scenarios considered and how the parameters differ relative to the Base model. Here we consider alternatives to existing levels of NPI, vaccines efficacy, susceptibility, vaccine availability and level of contacts in schools.

medRxiv preprint doi: https://doi.org/10.1101/2020.09.22.20199174; this version posted September 23, 2020. The copyright holder for this preprint (which was not certified by peer review) is the author/funder, who has granted medRxiv a license to display the preprint in perpetuity.

It is made available under a CC-BY-ND 4.0 International license .

Parameter	Description	Base Value(s)	Source
J	demographic groups: (1) age-only, (2) age and essential workers	{0-4, 5-19, 20-39, 40-59, 60-74, 75+}, {0-4, 5-19, 20-39, 20-39*, 40-59, 40-59*, 60-74, 75+}	assumed
σ_{asym}	infection asymptomatic rate	0.16	Byambasuren et al. (2020)
δ	infection fatality rate (age-specific)	{6.7×10^{-6}, 2.5×10^{-5}, 0.0002, 0.002, 0.018, 0.12}	Levin et al. (2020)
s	susceptibility (age-specific)	{0.5, 0.5, 1.0, 1.0, 1.0, 1.0}	Davies et al. (2020)
τ_{pre} τ_{asym} τ_{sym}	relative infectiousness by symptom type	0.51 0.51 1.0	Abrams et al. (2020)
D_{exp} D_{pre} D_{asym} D_{sym}	symptom duration (days)	3.0 3.2 3.5 7.0	Abrams et al. (2020)
ϵ	vaccine efficiency (age-specific)	{0.65, 0.65, 0.65, 0.65, 0.65, 0.65}	informed by influenza vaccine efficiency (Ohmit et al., 2014; McLean et al., 2015; Gaglani et al., 2016)
p	proportion of essential workers	0.49	calculated with labor data (Bartik et al., 2020; LMI and C2ER, 2020); alternative: (McCormack et al., 2020)
R_0	secondary infections in a naive population	2.5	Kucharski et al. (2020), Korevaar et al. (2020)
q	transmission probability in a naive population	0.053	calculated given R_0, s and other parameters
θ	scaling factor for transmission probability due to NPI other than social distancing	0.65	assumed (consistent with estimated COVID-19 R_0 under NPIs (Korevaar et al., 2020))
n	population shares: (1) age-only, (2) age and essential workers	{0.06, 0.19, 0.27, 0.26, 0.19, 0.04}, {0.06, 0.19, 0.19, 0.08, 0.18, 0.8, 0.19, 0.04}	Population Pyramid (2020)
e	remaining years of life expectancy (age-specific)	{76, 66, 50, 31, 17, 6}	USSSA (2020)
$I_{pre}(0)$ $I_{asym}(0)$ $I_{sym}(0)$ $R(0)$	initial pre-sympt. initial asymptomatic initial symptomatic initial recovered	$0.005n$ $0.005n$ $0.01n$ $0.09n$	IHME (2020a) estimates and projections
v	fraction of population vaccinated daily	0.1/30	informed by comments from CDC Director to U.S. Senate Panel (Lovelace Jr. and Higgins-Dunn, 2020)

Table 2: Base model parameter values and sources.

medRxiv preprint doi: https://doi.org/10.1101/2020.09.22.20199174; this version posted September 23, 2020. The copyright holder for this preprint (which was not certified by peer review) is the author/funder, who has granted medRxiv a license to display the preprint in perpetuity.

It is made available under a CC-BY-ND 4.0 International license .

Scenario	Change from Base scenario parameters	Source
Strong NPI	$\theta = 0.5$	assumed
Weak NPI	$\theta = 0.75$	consistent with 30-70% of U.S. population always wearing a mask (Premise, 2020) with 33-58% effectiveness (IHME, 2020b)
Weak vaccine	$\epsilon_i \in \{0.4, 0.4, 0.4, 0.4, 0.4\}$	informed by influenza vaccine efficiency
Weak vaccine seniors	$\epsilon_i \in \{0.65, 0.65, 0.65, 0.65, 0.5, 0.5\}$	informed by influenza vaccine efficiency
Low susceptibility ages < 20	$s_i \in \{0.34, 0.4, 1.0, 1.0, 1.0\}$	Zhang et al. (2020)
Even susceptibility	$s_i \in \{1.0, 1.0, 1.0, 1.0, 1.0\}$	assumed
Ramp up	$v(t) = \begin{cases} 0.05/30, & t \leq 90 \\ 0.15/30, & t > 90 \end{cases}$	informed by comments from the scientific head of the U.S. vaccine development program (Slaoui, 2020)
Open schools	$\alpha_{school} = 0.7$	assumed

Table 3: Parameter values that differ from the Base case for alternative scenarios.

4 Vaccine prioritization optimization

The planner's decision problem is to allocate the daily supply of vaccine ($v(t)$) across the demographic groups according to a given objective. We assume that this allocation vector, μ, can be chosen monthly at the beginning of each of the first six decision periods (e.g., monthly basis). We numerically solved for vaccine allocation strategies that minimize the total burden associated with three different health metrics: deaths (12), years of life lost (YLL) (13) or symptomatic infections (14):

$$\text{deaths: } \min \left\{ \int_0^T \sum_{i \in J} I_{sym,i}(t)/D_{sym} dt \right\} \tag{12}$$

$$\text{YLL: } \min \left\{ \int_0^T \sum_{i \in J} e_i \delta_i I_{sym,i}(t)/D_{sym} dt \right\} \tag{13}$$

$$\text{symptomatic infections: } \min \left\{ \int_0^T \sum_{i \in J} \delta_i I_{sym,i}(t)/D_{sym} dt \right\}, \tag{14}$$

where e_i is the years remaining of life expectancy for age group i and with a 6-month time horizon ($T = 180$ days). Preventing deaths and years of life lost are "consensus value(s) across expert reports" (Emanuel et al., 2020, p. 2052) while "protecting public health during the COVID-19 pandemic requires...minimizing COVID-19 infection" (Toner et al., 2020, p. 10).

We solved for the optimal allocation of available vaccines across demographic groups for each month over six months. We identified the optimal solution using a two-step algorithm. In the first step we used a genetic algorithm similar to (Patel et al., 2005) to identify an approximate solution. This approach uses random sampling of the

medRxiv preprint doi: https://doi.org/10.1101/2020.09.22.20199174; this version posted September 23, 2020. The copyright holder for this preprint (which was not certified by peer review) is the author/funder, who has granted medRxiv a license to display the preprint in perpetuity.

It is made available under a CC-BY-ND 4.0 International license .

potential solution space to broadly explore in order to avoid narrowing to a local and not global minimum. In the second step we used simulated annealing to identify the solution with precision. At a given optimal solution, it may or may not be the case that the outcome of interest (e.g. minimizing deaths) is sensitive to small changes in the allocation decision. Thus, around the optimal allocation we also identified nearby allocations that produce outcomes that are less desirable but still within 0.25% of the optimized outcome. A detailed description of the algorithm is given in the SI Appendix. All code for the optimization was written in the Julia programming language (Bezanson et al., 2017).

5 Results

We present results for the Base model with essential worker demographic groups and then show the sensitivity of these results with respect to the alternative scenarios. Results for individual alternative scenarios are presented in detail in the SI Appendix. In Fig. 2 we show the optimal allocation of vaccines given each objective for the Base model with essential workers. The allocations are shown on a monthly basis for six decision periods and then cumulatively (in percent of vaccine and percent of group vaccinated). Broadly, we find that the optimal policy is very dynamic: specific groups are targeted each period and these targets shift over time. Furthermore, targeting is very narrow to start but then becomes less so as vaccines continue to roll out.

In general we also find that optimal dynamic allocation does not cover 100% of the susceptible population in any single demographic group before switching to another age group. Further, an allocation may initially prioritize one group, only vaccinate a fraction of the population and prioritize that group again two or more decision periods later. These features suggest that there are diminishing marginal returns to vaccinating individuals in any single group.

The whiskers on bars in Fig. 2 show the range of alternative allocations that still produce an outcome that is within 0.25% of the optimum. For example, in the first period of the top panel the whiskers show that some limited substitution in the allocation between groups d^*, f^* and h (but not others) can occur without a substantial reduction in the optimized outcome (minimizing deaths). In general, we find that these whiskers become more pronounced as periods progress. This shows that it becomes less critical to precisely follow the exact optimal allocation as vaccine coverage of the population expands. We also find that, even with targeting in specific decision periods, after six periods the percent vaccine allocated to each group and the percent of each group vaccinated (Fig. 2, final two columns) is more even across most—though not all—groups. Overall, we find that pre-school age children are substantially less targeted than most groups (conditional on having relative few contacts and lower susceptibility).

Across objectives there are substantial differences in which groups are targeted early on. When minimizing deaths, targeting progresses from older essential workers (40-59*), to the oldest (75+), to younger seniors (60-74), and then younger essential workers (20-39*). These groups are a mix of those at high risk of mortality (older groups) and high risk of contraction and spread (essential workers). When minimizing YLL, younger essential workers and younger seniors are targeted earlier (given their longer average years of life remaining). Finally, when minimizing infections we find that younger essential workers take top priority, followed by older essential workers and school-age children

medRxiv preprint doi: https://doi.org/10.1101/2020.09.22.20199174; this version posted September 23, 2020. The copyright holder for this preprint (which was not certified by peer review) is the author/funder, who has granted medRxiv a license to display the preprint in perpetuity.

It is made available under a CC-BY-ND 4.0 International license .

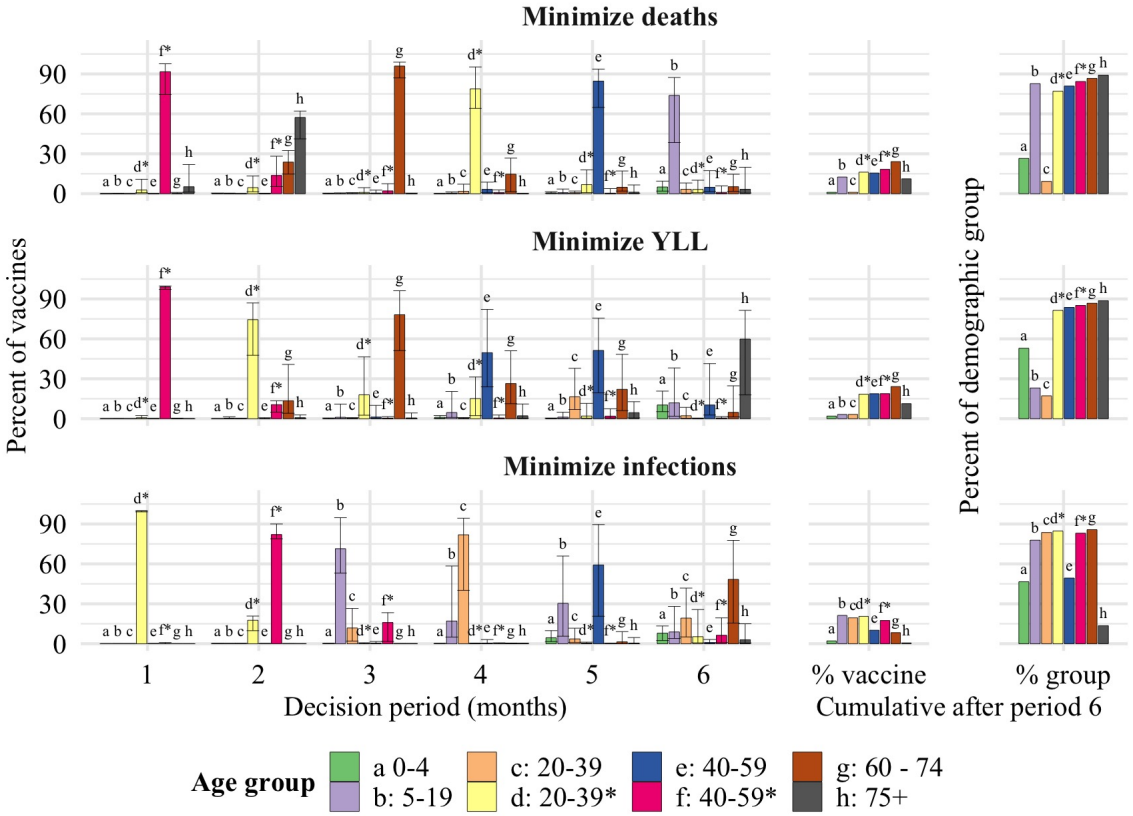

Figure 2: The optimal allocation of vaccines (vertical axes) between demographic groups for each decision period (horizontal axis) under the Base scenario in the essential worker model. The three rows represent each objective (from top to bottom): minimize deaths, minimize years of life lost (YLL) and minimize infections. The bars for the six decision periods show the percentage of vaccines allocated to a specific group (indicated by a letter, color, and asterisks for essential worker groups) in that period. The two final columns show cumulative measures at the end of month six: the percent of (1) vaccines allocated to each group, and (2) each group that has been vaccinated. The whiskers on each bar represent the sensitivity of the optimal solution to small deviations in the outcome, specifically the range of allocations resulting in outcomes within 0.25% of the optimal solution.

(5-19), since these groups have higher contacts and thus risk of contraction and spread.

Results for the age-only model—that does not distinguish essential workers—are broadly similar (see SI Appendix). However, a significant difference is that the essential worker formulation presented in the main text targets essential workers before other working age adults and prioritizes these groups before the higher risk 60+ age groups.

In the left panel of Fig. 3 we show the dynamic path of infections, starting from the period in which vaccines become available, under various policies. As expected, infections are highest given no vaccines. Results for allocating vaccines in a manner "proportional" to each group's size shows the substantial value of vaccines even with no targeting. As expected, the policy for minimizing infections leads to the lowest level of infections. In the second panel of Fig. 3 we show the performance of each targeting policy relative to outcomes achieved with a proportional allocation. Overall we find that when focusing on minimizing a particular outcome, that outcome is reduced by 17-18%. In the

medRxiv preprint doi: https://doi.org/10.1101/2020.09.22.20199174; this version posted September 23, 2020. The copyright holder for this preprint (which was not certified by peer review) is the author/funder, who has granted medRxiv a license to display the preprint in perpetuity.

It is made available under a CC-BY-ND 4.0 International license .

first cluster of bars, as expected the policy that minimizes deaths ("D" in green) leads to the greatest reduction in deaths (18%). However, trade offs are stark in certain cases: the third cluster of bars shows that minimizing deaths involves a strong opportunity cost in terms of infections, which are higher than even under the proportional policy. The YLL policy is most consistent, performing second best when considering other outcomes (infections and deaths).

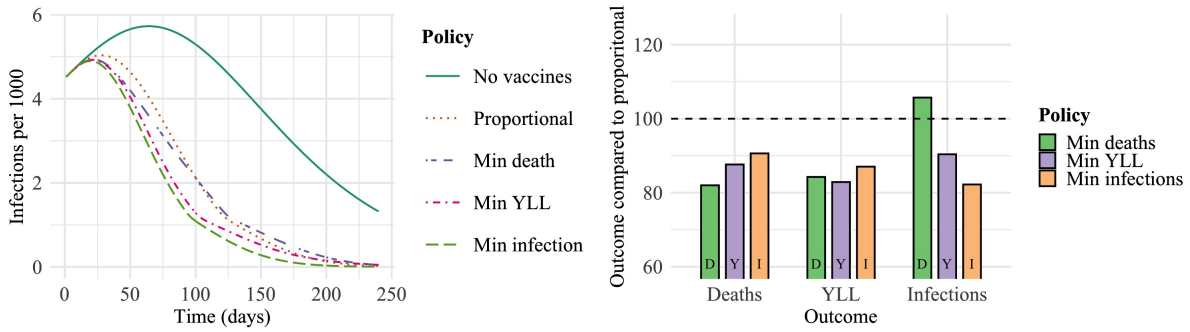

Figure 3: The number of infections per 1,000 individuals over time under each policy (left) and the performance of each policy relative to a uniform allocation policy (right) for the base scenario in the essential worker model. The bars are clustered by the resulting outcome and colored by the objective driving each policy.

5.1 Sensitivity of prioritization across scenarios

Iterations of Fig. 2 and Fig. 3 for all alternative scenarios are shown in the SI Appendix. To compare and contrast cumulative vaccination results, in Figure 4 we show for each of the alternative scenarios the percentage of each group vaccinated after three months (left panel) and 6 months (right panel). In general we find differences across groups that lessen (but not completely) by month six. We also find some differences across scenarios and objectives that differ by the horizon considered.

Certain scenarios are distinctive. For example, when the lower susceptibility enjoyed by those under 20 in the Base scenario is replaced by "Even susceptibility" for all, over the first three months we see substantial substitution to school age children and away from older essential workers (min. deaths or infections) or younger seniors (min. YLL). In a second example, both weaker vaccine scenarios do not substantially change results at three months, except if minimizing deaths, in which case vaccination shifts from younger seniors to younger essential workers. When fewer vaccines are available in the first three months due to a "Ramp up" in supply, the deficit mainly accrues to older essential workers (min. deaths or infections), younger seniors (min. deaths or YLL), younger essential workers (min. YLL), or school age children (min. infections).

At three months, the only two groups consistently *not* targeted are pre-school age children and older non-essential workers. By six months, there are two groups consistently targeted: older and younger essential workers. Across each objective, one of the essential worker groups has either the highest or second highest coverage rate. The only exception to this rule is if school age children are equally susceptible to infection as adults (as discussed above).

medRxiv preprint doi: https://doi.org/10.1101/2020.09.22.20199174; this version posted September 23, 2020. The copyright holder for this preprint (which was not certified by peer review) is the author/funder, who has granted medRxiv a license to display the preprint in perpetuity.

It is made available under a CC-BY-ND 4.0 International license .

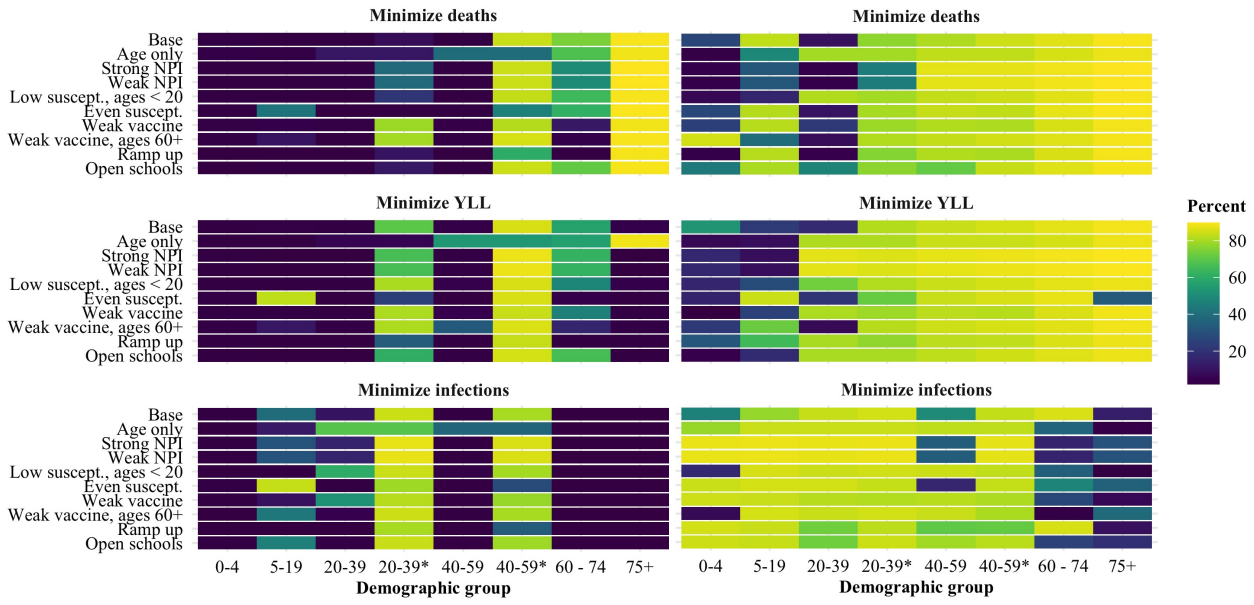

(a) Three months

(b) Six months

Figure 4: The cumulative percent of each demographic group (x-axis) vaccinated after three or six months under alternative scenarios (y-axis) and each objective (panel). Vaccine supply is sufficient to vaccinate 10% of the population each month, except in the "Ramp up" scenario which involves 5% per month for three months, then 15% per month.

5.2 Vaccines partially effective at the individual level

In our results discussed above we have assumed that for a given percentage of each group (e.g. 65%) vaccines are completely effective at preventing infection. An alternative approach is to consider vaccines as partially effective for everyone at the individual level. Furthermore, it may be the case that a vaccine is more effective at reducing symptoms than preventing infections. To analyze this case we extended our model structure to separate infected individuals into those that had not been vaccinated. For vaccinated individuals, we replaced the single vaccine efficacy parameter with separate parameters for reduction in spread (scaling susceptibility and transmissibility) and mortality (scaling infection fatality rate). We consider three cases. For comparison with the Base model, we consider the same level of efficacy (65%) for spread and mortality. We also consider a vaccine that is more effective at reducing mortality but less effective at preventing spread. Specifically we model an extreme case where the vaccine reduces susceptibility and infectiousness by 10% and infection fatality rate by 90% and a moderate case where these values were 30% and 70% respectively. Detail on modeling and results for these cases are provided in SI Appendix C.

In general, results are similar between the Base model with 65% of individuals 100% protected when vaccinated and the three scenarios we tested with the partially effective vaccine model formulation. However, when the cases where the vaccine had an efficacy of 65% for susceptibility, infectiousness and mortality, and when the vaccine had an efficacy of 90% against mortality but only 10% against susceptibility and infectiousness, the optimal solutions allocated a greater share of vaccines to ages 60+ to minimize years of life lost and deaths compared to the Base

medRxiv preprint doi: https://doi.org/10.1101/2020.09.22.20199174; this version posted September 23, 2020. The copyright holder for this preprint (which was not certified by peer review) is the author/funder, who has granted medRxiv a license to display the preprint in perpetuity.

It is made available under a CC-BY-ND 4.0 International license .

model. Surprisingly, the scenario with a vaccine the reduces mortality by 70% and susceptibility and infectiousness by 30% was qualitatively different to the others, shifting prioritization towards younger essential workers and away from older nonessential workers. This finding illustrates that the indirect benefits of reducing spread (e.g. in younger essential workers) is still an important driver relative to the direct benefits of reducing mortality (e.g. in older non-essential workers) even given a vaccine that is relatively less effective at mitigating infections.

6 Discussion

Key insights and results from our analysis are summarized in Box 1. Together these lessons show the strong implications of considering dynamic solutions, social distancing and essential workers (given their limitations in social distancing) for vaccine prioritization.

Box 1. Key insights and results

1. **Benefits:** Prioritization can reduce a particular undesirable outcomes (deaths, YLL, or infections), by 17-18% in the Base scenario (or 8-23% depending on the alternative scenario).
2. **Dynamic prioritization:** (A) Prioritization is responsive to the initial and evolving disease status; (B) Diminishing marginal returns to additional vaccination within a group drives a shift to other groups well before 100% vaccination of the first group is achieved.
3. **High prioritization:** Under the Base scenario, group prioritization over the first three months starts with essential workers then, depending on the objective, progresses to older and younger seniors (deaths), younger seniors only (YLL) or school age children (infections).
4. **Low prioritization:** At three months (30% of the population vaccinated) the only two groups consistently *not* targeted are pre-school age children and older non-essential workers.
5. **Widening prioritization:** As vaccination rates rise, precise prioritization becomes less critical and targeting widens to a larger set of groups.
6. **Sensitivity:** Some prioritization results are sensitive to the scenario modeled—especially whether or not those under 20 are less susceptible.
7. **Trade offs:** Focusing on one objective leads to sacrifices in the other objectives, typically strongest when minimizing infections.

While vaccine prioritization discussion often takes the form of identifying tiers that should be vaccinated to completion before moving on (e.g. see Toner et al. 2020, p. 25), we find that the optimal approach does not involve seeking 100% coverage in a single group before prioritizing other groups. In fact, in some cases a group is prioritized early on, and then revisited two or more periods later. These findings are indicative of the diminishing marginal returns to vaccinating individuals within a demographic group. Because social contacts are concentrated within groups, as vaccine coverage in a given group increases, risks for that group fall more sharply than for others. Thus, as group vaccine coverage increases, we see attenuation in the direct benefits (protection of the vaccinated) and indirect benefits (protection of the unvaccinated) of additional vaccinations in that group.

Available existing analysis of optimal COVID-19 vaccination targeting in preprint form is limited to Matrajt et al. (2020) and Bubar et al. (2020). Before comparing and contrasting results some key modeling differences should be noted. Both preprints consider a wider range of vaccine availability than considered here. Their models do not

medRxiv preprint doi: https://doi.org/10.1101/2020.09.22.20199174; this version posted September 23, 2020. The copyright holder for this preprint (which was not certified by peer review) is the author/funder, who has granted medRxiv a license to display the preprint in perpetuity.

It is made available under a CC-BY-ND 4.0 International license .

incorporate non-pharmaceutical interventions (NPIs), including social distancing and non-social distancing (e.g. mask wearing) as we do here. Doing so allows us to account for differences between groups like essential workers constrained in distancing versus others who are much less so. Matrajt et al. (2020) and Bubar et al. (2020) both implement static optimization where all vaccination available is allocated and administered in a one-shot process. Our allocation is dynamic, responding to changing conditions over a six-month period. Finally, Matrajt et al. (2020) and Bubar et al. (2020) model vaccines as "leaky", i.e., reducing the probability that a susceptible individual will be infected. Bubar et al. (2020) also considers an "all-or-nothing" vaccine that 100% effective for a fraction of the population. In our Base model the vaccine is "all-or-nothing", though we check our results against a leaky vaccine in the SI Appendix..

Matrajt et al. (2020) found that optimal strategies to minimize deaths and years of life lost will either exclusively target groups with high infection fatality rates maximizing the direct benefit of vaccines, or will target groups with high rates of infection maximizing the indirect benefits of the vaccine. In contrast, our results indicate that optimal policies initially target groups with high risk of infection and switch to targeting groups with high infection fatality. This difference is most likely follows from our dynamic versus static allocation. The switching behavior we identify is consistent with past work on pandemic influenza vaccine prioritization, which suggests that early in an outbreak when the infection rate is growing targeting spread (maximizing indirect benefits) is more efficient, but later when the infection rate is leveling off or declining maximizing direct protection is most efficient (Matrajt et al., 2013). Consistent with this explanation, we find that ages 75+ yrs. are prioritized in the first decision period when deaths are minimized in the strong NPI scenario where the number of infections are declining, compared to the base case where they are not prioritized until the second period.

Bubar et al. (2020) found that prioritizing adults older than 60 years of age is a robust strategy for minimizing deaths. In contrast we find that working age adults are a key priority group, particularly essential workers between the ages of 40 and 59 yrs. These differences may either arise from differences in social distancing or dynamic allocation. Our accounting for social distancing on COVID-19 transmission increases the modeled benefits of targeting essential workers, who are less able to substantially reduce their social contacts than individuals ages 60+. Furthermore, as discussed above, the ability of dynamic polices to switch over time allows the allocating schemes we discuss to capture the benefits of using the initial vaccine supply to slow transmission without sacrificing direct protection of more vulnerable individuals later on.

While we explored a large set of alternative scenarios, there are other important possibilities that we have not included. For example, if certain population groups (e.g., children or seniors) experience significant side effects from the vaccine, prioritization might shift away from these groups (NASEM, 2020). Another key component is the set of logistical constraints imposed by the distribution network used. Vaccines will likely be administered through various points of contact with the community (pharmacies, clinics, schools, etc.). For some demographic groups there may be differences between the share of vaccines targeted to that group and the actual share received, e.g., due to constraints in prediction and implementation.

We do not address the potential for vaccine hesitancy in the model. In general, we find that it is not necessary

medRxiv preprint doi: https://doi.org/10.1101/2020.09.22.20199174; this version posted September 23, 2020. The copyright holder for this preprint (which was not certified by peer review) is the author/funder, who has granted medRxiv a license to display the preprint in perpetuity.

It is made available under a CC-BY-ND 4.0 International license .

or even ideal to vaccinate all of the susceptible individuals in a demographic group, at least among the first 60% of the population vaccinated as we consider here. Thus, at least initially, some level of vaccine hesitancy may not have a material impact. However, hesitancy may play a more significant role in the longer run, especially if hesitancy rates are large and herd immunity proves difficult to achieve (e.g. if vaccine efficacy is low, and/or NPI relaxation is aggressive). Vaccine hesitancy that is concentrated in a particular community or demographic group could also motivate changing a prioritization strategy. Similarly, adjustments would be needed if groups differ in the duration of vaccine efficacy or diligence in obtaining a second dose of the vaccine (as necessary).

For simplicity we limited policy objectives to a set of concise metrics of health outcomes (minimizing expected cases, years of life lost, or deaths). However, other health-related metrics such as protecting the most vulnerable and social values such returning to school, work and social life are important to consider. Our analysis reveals that optimal strategies for minimizing deaths and years of life lost are broadly aligned with the goal of protecting the most vulnerable. These solution target essential workers who are the least able to participate in NPI such as social distancing and thus are the most a risk of infection, and individuals over the age of 60 who have the highest risk of deaths if infected by the disease. Other social values such as returning to school will most likely change the allocation schemes to offset the risk created by relaxing social distancing. For example, if allowing children to return to school was a high priority, then allocation strategies might be tilted towards targeting school age children and teachers. A detailed analysis of optimal vaccine allocation given the relaxation of social distancing to achieve particular social objectives is a potentially promising direction for future research.

Acknowledgements

We thank participants in the MIDAS network COVID-19 modeling seminar for helpful comments. This research was supported by an Emergency COVID-19 Seed Award from the California Breast Cancer Research Program of the University of California (UC), Grant Number R00RG2419. GC is partially support by NSF grants 2026797, 2034003, and NIH R01 GM 130900. This material is based upon work supported by the National Science Foundation Graduate Research Fellowship Program under Grant No. 1650042. Any opinions,findings, and conclusions or recommendations expressed in this material are those of the authors and do not necessarily reflect the views of the National Science Foundation

References

Abrams, S., J. Wambua, E. Santermans, L. Willem, E. Kuylen, P. Coletti, P. Libin, C. Faes, O. Petrof, S. A. Herzog, The SIMID COVID-19 team, P. Beutels, and N. Hens (2020, July). Modeling the early phase of the Belgian COVID-19 epidemic using a stochastic compartmental model and studying its implied future trajectories. preprint, medRxiv, doi: 10.1101/2020.06.29.20142851.

Bartik, A. W., Z. B. Cullen, E. L. Glaeser, M. Luca, and C. T. Stanton (2020). What jobs are being done at home during the COVID-19 crisis? Evidence from firm-level surveys. National Bureau of Economic Research Working Paper No. 27422.

medRxiv preprint doi: https://doi.org/10.1101/2020.09.22.20199174; this version posted September 23, 2020. The copyright holder for this preprint **(which was not certified by peer review)** is the author/funder, who has granted medRxiv a license to display the preprint in perpetuity.

It is made available under a CC-BY-ND 4.0 International license .

Bezanson, J., A. Edelman, S. Karpinski, and V. B. Shah (2017). Julia: A fresh approach to numerical computing. *SIAM Review 59*(1), 65–98.

Bubar, K. M., S. M. Kissler, M. Lipsitch, S. Cobey, Y. Grad, and D. B. Larremore (2020, Sept). Model-informed COVID-19 vaccine prioritization strategies by age and serostatus. preprint, medRxiv, doi: 10.1101/2020.09.08.20190629.

Byambasuren, O., M. Cardona, K. Bell, J. Clark, M.-L. McLaws, and P. Glasziou (2020). Estimating the extent of true asymptomatic COVID-19 and its potential for community transmission: systematic review and meta-analysis. *Available at SSRN 3586675*.

Chowell, G., C. Viboud, X. Wang, S. M. Bertozzi, and M. A. Miller (2009). Adaptive vaccination strategies to mitigate pandemic influenza: Mexico as a case study. *PLoS One 4*(12), e8164.

Circella, G. (2020). The COVID-19 pandemic: What does it mean for mobility? What the temporary vs. longer-term impacts? UC Davis Institute for Transportation Studies webinar, `https://app.box.com/s/ybygjz94f855rg4lex06dsnq61v530t2/file/691630702422`.

Corey, L., J. R. Mascola, A. S. Fauci, and F. S. Collins (2020). A strategic approach to COVID-19 vaccine R&D. *Science 368*(6494), 948–950.

Davies, N. G., P. Klepac, Y. Liu, K. Prem, M. Jit, CMMID COVID-19 working group, and R. M. Eggo (2020). Age-dependent effects in the transmission and control of COVID-19 epidemics. *Nature Medicine 26*, 1205–1211.

Dong, E., H. Du, and L. Gardner (2020). An interactive web-based dashboard to track COVID-19 in real time. *The Lancet Infectious Diseases 20*(5), 533–534.

Emanuel, E., G. Persad, R. Upshur, B. Thome, M. Parker, A. Glickman, C. Zhang, C. Boyle, M. Smith, and J. Phillips (2020). Fair allocation of scarce medical resources in the time of Covid-19. *The New England Journal of Medicine 382*, 2049–2055.

Erman, M. and J. Mason (2020, Aug). Fauci expects tens of millions of coronavirus vaccine doses at start of 2021. *Reuters*.

Gaglani, M., J. Pruszynski, K. Murthy, L. Clipper, A. Robertson, M. Reis, J. R. Chung, P. A. Piedra, V. Avadhanula, M. P. Nowalk, et al. (2016). Influenza vaccine effectiveness against 2009 pandemic influenza a (H1N1) virus differed by vaccine type during 2013–2014 in the United States. *The Journal of Infectious Diseases 213*(10), 1546–1556.

Gallagher, M. E., A. J. Sieben, K. N. Nelson, A. N. Kraay, B. Lopman, A. Handel, and K. Koelle (2020, Aug). Considering indirect benefits is critical when evaluating sars-cov-2 vaccine candidates. preprint, medRxiv, doi: 10.1101/2020.08.07.20170456.

Institute for Health Metrics and Evaluation (IHME) (2020a). Covid-19 mortality, infection, testing, hospital resource use, and social distancing projections (August 21, 2020 estimates). Seattle, United States of America: Institute for Health Metrics and Evaluation (IHME), University of Washington, `https://ihmecovid19storage.blob.core.windows.net/latest/ihme-covid19.zip`.

Institute for Health Metrics and Evaluation (IHME) (2020b). COVID-19: What's new for June 25, 2020. Seattle, United States of America: Institute for Health Metrics and Evaluation (IHME), University of Washington, `https://www.healthdata.org/sites/default/files/files/Projects/COVID/Estimation_update_062520.pdf`.

Korevaar, H. M., A. D. Becker, I. F. Miller, B. T. Grenfell, C. J. E. Metcalf, and M. J. Mina (2020). Quantifying the impact of US state non-pharmaceutical interventions on COVID-19 transmission. medRxiv [Preprint]. July 1, 2020. Available from: `https://doi.org/10.1101/2020.06.30.20142877`.

Kucharski, A. J., T. W. Russell, C. Diamond, Y. Liu, J. Edmunds, S. Funk, R. M. Eggo, F. Sun, M. Jit, J. D. Munday, N. Davies, A. Gimma, K. v. Zandvoort, H. Gibbs, J. Hellewell, C. I. Jarvis, S. Clifford, B. J. Quilty, N. I. Bosse, S. Abbott, P. Klepac, and S. Flasche (2020). Early dynamics of transmission and control of COVID-19: a mathematical modelling study. *The Lancet Infectious Diseases 20*(5), 553 – 558.

Levin, A. T., K. B. Cochran, and S. P. Walsh (2020). Assessing the age specificity of infection fatality rates for COVID-19: Meta-analysis & public policy implications. National Bureau of Economic Research Working Paper No. 27597.

medRxiv preprint doi: https://doi.org/10.1101/2020.09.22.20199174; this version posted September 23, 2020. The copyright holder for this preprint **(which was not certified by peer review)** is the author/funder, who has granted medRxiv a license to display the preprint in perpetuity.

It is made available under a CC-BY-ND 4.0 International license .

LMI and C2ER (2020). SOC codes for CISA critical infrastructure workers. data retrieved from LMI institute webstite, `https://www.lmiontheweb.org/more-than-half-of-u-s-workers-in-critical-occupations-in-the-fight-against-covid-19/`.

Lovelace Jr., B. and N. Higgins-Dunn (2020, Sept). CDC says U.S. should have enough coronavirus vaccine to return to "'regular life"' by third quarter of 2021. *cnbc.com*.

Lurie, N., M. Saville, R. Hatchett, and J. Halton (2020). Developing Covid-19 vaccines at pandemic speed. *New England Journal of Medicine 382*(21), 1969–1973.

Matrajt, L., J. Eaton, T. Leung, and E. R. Brown (2020, Aug). Vaccine optimization for COVID-19, who to vaccinate first? preprint, medRxiv, doi: 10.1101/2020.08.14.20175257.

Matrajt, L., M. E. Halloran, and I. M. Longini Jr (2013). Optimal vaccine allocation for the early mitigation of pandemic influenza. *PLoS Comput Biol 9*(3), e1002964.

McCormack, G., C. Avery, A. K.-L. Spitzer, and A. Chandra (2020). Economic vulnerability of households with essential workers. *JAMA 324*(4), 388–390.

McLean, H. Q., M. G. Thompson, M. E. Sundaram, B. A. Kieke, M. Gaglani, K. Murthy, P. A. Piedra, R. K. Zimmerman, M. P. Nowalk, J. M. Raviotta, et al. (2015). Influenza vaccine effectiveness in the United States during 2012–2013: variable protection by age and virus type. *The Journal of Infectious Diseases 211*(10), 1529–1540.

Medlock, J. and A. P. Galvani (2009). Optimizing influenza vaccine distribution. *Science 325*(5948), 1705–1708.

National Academies of Sciences, Engineering, and Medicine (2020). Discussion draft of the preliminary framework for equitable allocation of COVID-19 vaccine. Washington, DC: The National Academies Press. `https://doi.org/10.17226/25914`.

Ohmit, S. E., M. G. Thompson, J. G. Petrie, S. N. Thaker, M. L. Jackson, E. A. Belongia, R. K. Zimmerman, M. Gaglani, L. Lamerato, S. M. Spencer, et al. (2014). Influenza vaccine effectiveness in the 2011–2012 season: protection against each circulating virus and the effect of prior vaccination on estimates. *Clinical Infectious Diseases 58*(3), 319–327.

Patel, R., I. M. Longini Jr, and M. E. Halloran (2005). Finding optimal vaccination strategies for pandemic influenza using genetic algorithms. *Journal of Theoretical Biology 234*(2), 201–212.

Population Pyramid (2020). Population of the United States. `https://www.populationpyramid.net`, accessed July 12, 2020.

Prem, K., A. R. Cook, and M. Jit (2017). Projecting social contact matrices in 152 countries using contact surveys and demographic data. *PLoS Computational Biology 13*(9), e1005697.

Premise (2020). How mask-wearing has changed in America: A visual journey of increasing mask use. San Francisco, United States of America: Premise.com, `https://www.premise.com/how-mask-wearing-has-changed-in-america-a-visual-journey-of-increasing-mask-use/`.

Slaoui, M. (2020, Sept). Interview with Mary Louise Kelly: Operation Warp Speed top adviser on the status of a coronavirus vaccine. *National Public Radio*.

Toner, E., A. Barnill, C. Krubiner, and et al. (2020, August). Interim framework for COVID-19 vaccine allocation and distribution in the United States. Baltimore, MD: Johns Hopkins Center for Health Security, `https://www.centerforhealthsecurity.org/our-work/pubs_archive/pubs-pdfs/2020/200819-vaccine-allocation.pdf`.

U.S. Department of Health and Human Services (USHSS) (2020). Witnesses appearing before the House Select Subcommittee on Coronavirus Crisis. Hearing: The urgent need for a national plan to contain the coronavirus. `https://docs.house.gov/meetings/VC/VC00/20200731/110912/HHRG-116-VC00-Wstate-FauciA-20200731.pdf`.

U.S. Social Security Administration (USSSA) (2020). Life Table. Data retrieved from USSSA website, `https://www.ssa.gov/oact/STATS/table4c6.html`.

Van Kerckhove, K., N. Hens, W. J. Edmunds, and K. T. Eames (2013). The impact of illness on social networks: implications for transmission and control of influenza. *American Journal of Epidemiology 178*(11), 1655–1662.

medRxiv preprint doi: https://doi.org/10.1101/2020.09.22.20199174; this version posted September 23, 2020. The copyright holder for this preprint **(which was not certified by peer review)** is the author/funder, who has granted medRxiv a license to display the preprint in perpetuity.

It is made available under a CC-BY-ND 4.0 International license .

Verity, R., L. C. Okell, I. Dorigatti, P. Winskill, C. Whittaker, N. Imai, G. Cuomo-Dannenburg, H. Thompson, P. G. Walker, H. Fu, et al. (2020). Estimates of the severity of coronavirus disease 2019: a model-based analysis. *The Lancet Infectious Diseases*.

Weill, J. A., M. Stigler, O. Deschenes, and M. R. Springborn (2020). Social distancing responses to COVID-19 emergency declarations strongly differentiated by income. *Proceedings of the National Academy of Sciences 202009412*.

Zhang, J., M. Litvinova, Y. Liang, Y. Wang, W. Wang, S. Zhao, Q. Wu, S. Merler, C. Viboud, A. Vespignani, et al. (2020). Changes in contact patterns shape the dynamics of the COVID-19 outbreak in china. *Science 368*(6498), 1481–1486.

medRxiv preprint doi: https://doi.org/10.1101/2020.09.22.20199174; this version posted September 23, 2020. The copyright holder for this preprint (which was not certified by peer review) is the author/funder, who has granted medRxiv a license to display the preprint in perpetuity.

It is made available under a CC-BY-ND 4.0 International license .

Appendix

A Model specification, parameterization and optimization

A.1 Initial conditions

We set plausible baseline values for initial epidemiological conditions that will be present in the U.S. population when a vaccine arrives using estimates of actual U.S. cases from the start of the outbreak (February 2020) through present and expected cases projected forward through December 1, 2020 produced by the Institute for Health Metrics and Evaluation (IHME, 2020a). For the share of the population that is symptomatic, $I_{sym}(0)$, we take the estimated case count for the $D_{sym} = 7$ days (the duration of symptomatic infection) ending December 1, 2020, multiply by the share of cases that are symptomatic $(1 - \sigma_{asym})$ and then divide by the U.S. population. For the pre-symptomatic share, $I_{pre}(0)$, we assume it is consistent with $I_{sym}(0)$ but scaled by its shorter duration: $I_{pre}(0) = I_{sym}(0) * \left(\frac{D_{pre}}{D_{sym}}\right)$. The asymptomatic share is calculated by scaling $I_{sym}(0)$ to account for differences in duration and the relative share of asymptomatic to symptomatic cases: $I_{asym}(0) = I_{sym}(0) * \left(\frac{D_{asym}}{D_{sym}}\right) * \left(\frac{\sigma_{asym}}{1-\sigma_{asym}}\right)$. Finally, we estimate the share of the population that is recovered, $R(0)$, by taking the cumulative projected case count through December 1, 2020, divided by the total population.

A.2 Contact matrices distinguishing essential workers

Estimated contact rates for the U.S. were obtained from Prem et al. (2017) who used population-based contact diaries from the European POLYMOD survey to project to other countries, including the U.S. These included contact rates for 16 age classes in five year increments from ages 0 to 80. We collapsed these to five age groups (0-4, 5-19, 20-39, 40-59, 60-80) using population-weighted sums:

$$\hat{r}_{i,j,x} = \sum_{\mathtt{i} \in i} \left(\frac{N^{pop}_{\mathtt{i}}}{N^{pop}_{i}} \sum_{\mathtt{j} \in j} r_{\mathtt{i},\mathtt{j},x} \right), \tag{15}$$

where $\{\mathtt{i}, \mathtt{j}\}$ are the subscripts for the five year age bins, $\{i, j\}$ are the subscripts for the larger age bins, $r_{\mathtt{i},\mathtt{j},x}$ is the average number of daily contacts a person in group $\mathtt{i}$ makes with a person in group $\mathtt{j}$ for activity/location x, and N^{pop}_{h} is the population size for age group h.

The total number of i-to-j contacts must equal the total number of j-to-i contacts: $N^{pop}_{i} r_{i,j,x} = N^{pop}_{j} r_{j,i,x}$. Because numerical issues—estimation in Prem et al. (2017), bin discretization and rounding—can lead to small differences, we ensure this condition holds by imposing,

$$r_{i,j,x} = \frac{0.5(N^{pop}_{i} \hat{r}_{i,j,x} + N^{pop}_{j} \hat{r}_{j,i,x})}{N^{pop}_{i}}, \tag{16}$$

where the numerator is the mean of the two measures of total contacts between groups i and j and the denominator transforms the result to per-capita in i.

Setting essential worker contact rates requires additional assumptions and attention to the activity/location. We define the essential worker indicators $e \in \{n, y\}$ for "no" and "yes". Our grouping is such that all essential workers $(e = y)$ are employed but non-essential-workers $(e = n)$ are a mix of employed and not employed. Let e' represent the indicator for a second group which can be equal or not equal to the value for e.

In the case of all activities/locations x that are not *work*, contact rates are given by

$$r_{(i,\mathtt{e}),(j,e'),x} = \frac{N^{pop}_{(j,e')}}{N^{pop}_{j}} r_{i,j,x}, \quad \forall\, x \neq work. \tag{17}$$

This follows from the assumption that contacts made by any group (i, e) with any other group (j, e') are independent of i's essential worker status. Thus, we only need to split contacts $r_{i,j,x}$ into those made with essential worker type $e' = y$ versus the remainder with type $e' = n$, i.e. given the share $N^{pop}_{(j,e')}/N^{pop}_{j}$.

Estimating contacts when $x = work$ involves a larger number of steps. We first address contacts made by essential workers $(e = y)$ before turning to non-essential workers $(e = n)$. For $e = y$, let the share of the working age population $(20 - 59)$ in group i that is employed be given by p_i.

We assume that all of the work contacts are attributable to employed adults resulting in an employed adult

medRxiv preprint doi: https://doi.org/10.1101/2020.09.22.20199174; this version posted September 23, 2020. The copyright holder for this preprint (which was not certified by peer review) is the author/funder, who has granted medRxiv a license to display the preprint in perpetuity.

It is made available under a CC-BY-ND 4.0 International license .

contact rate of $r_{i,j,work}/p_i$. Then the contact rate of essential workers ($e = y$) in group i with age group j is

$$r_{(i,y),j,work} = \frac{r_{i,j,work}}{p_i}. \tag{18}$$

Let the fraction of working age group i that is employed in an essential worker role be given by $p_{i,y}$. The average workplace contact rate for non-essential-workers in group i with group j is given by

$$r_{(i,n),j,work} = \alpha_{work} \left(\frac{r_{i,j,work}}{p_i} \right) \left(\frac{p_i - p_{i,y}}{1 - p_{i,y}} \right), \tag{19}$$

where $\alpha_{work} < 1$ scales for social distancing and the final term in brackets scales for the share of non-essential workers that are employed and thus have contacts at $work$.

Finally, we assume that the average $work$place contact rate for an individual of type (i, e) with individuals of type (j, e') is given by the partial contact rate $r_{(i,e),j,work}$ times the proportion of total work contacts of individuals in group j that are made by individuals in sub group e':

$$r_{(i,e),(j,e'),work} = r_{(i,e),j,work} \left(\frac{N_{(j,e')} \cdot r_{i,(j,e'),work}}{N_{(j,y)} \cdot r_{i,(j,y),work} + N_{(j,n)} \cdot r_{i,(j,n),work}} \right). \tag{20}$$

Finally we scale the work contacts for age groups that are not separated into essential and non-essential workers (5-19, 60-80) to match the scaling for prime working age classes.

$$r_{i,j,work} = \left(\frac{p_{i,y}}{p_{work}} + \alpha \frac{p_{work} - p_{i,y}}{p_{work}} \right) r_{i,j,work} \tag{21}$$

A.3 Optimization algorithm

The optimization algorithm used our analysis is split into two parts. First a genetic algorithm is run to identify an effective strategy near a global optimum. This solution is then refined using simulated annealing algorithm.

Genetic algorithms take inspiration from the natural process of evolution, and work by randomly sampling a populating of candidate solutions, selecting a set of survivors based on the candidates performance against the objective function, information from these survivors is then used to generate a new generation of candidates solutions, and so forth (Patel et al., 2005). The genetic algorithm executes the following steps:

1. Sample $N_{t=0}$ candidate solutions $\{x_{n,t=0}\}$ from a Dirichlet distribution with parameter α_0.
2. Each candidate solution is evaluated with the objective function.
3. The bests $K_{t=0}$ candidates $\{x^{best}_{n,t=0}\}$ are solved and the distributions parameter α_0 is updated to α_1 by maximizing the likelihood of of the $\{x^{best}_{n,t=0}\}$.
4. Steps 1 to 3 are repeated for a fixed number of iterations T and the best candidate solution sampled at any iteration is returned. The values N_t and K_t are tuned for each step to maximize performance.

Simulated annealing is based on thermodynamic models of cooling metals. Briefly, the algorithm is initialized by sampling a candidate solution x_0, this candidate solution is updated by sampling a new candidate solution x_t from a proposal distribution centered around x_0. This solution is either accepted and replaces the current x_0 or it is rejected and a new candidate solution is drawn using the existing value of x_0. The proposed solutions x_t are accepted if they perform better against the objective than the incumbent x_0, if $x_t > x_0$ it is selected with probability $p = exp\left[-(x_t - x_0)/T_t\right]$. large values of T_t increase the probability that a new candidate solution will be accepted allowing the algorithm to explore the solution space and move away from local minima. T_t is reduced over time to allow the algorithm to start exploring the solution space and then eventually stabilize on a global minimum. The simulated annealing executes the following steps:

1. Initialize a chain with value x_0. Generate a new sample from the proposal distribution $x_t \sim tr(N(tr^{-1}(x_0), \sigma I))$ where the transform tr from $\mathbf{R}^n$ to the solution space. Initialize a counter i that track the number of iterations.
2. If $x_t < x_0$ replace x_0 with x_t, update $i = i + 1$ and repeat from step 1.
3. If $x_t > x_0$ sample $\mu \sim unif(0, 1)$. If $\mu > exp\left(-(x_t - x_0)/T(i)\right)$ then replace x_0 with x_t update i and repeat from step 1. Other wise save x_0 and repeat from step 1. We used $T(i) = T_0/i$ as the temperature function.
4. Stop when $i > max_iter$

These algorithms were tuned experimentally to consistently converge on a minimum solution on a test case. We used the minimum years of life lost under the base parameter set as our test case.

medRxiv preprint doi: https://doi.org/10.1101/2020.09.22.20199174; this version posted September 23, 2020. The copyright holder for this preprint (which was not certified by peer review) is the author/funder, who has granted medRxiv a license to display the preprint in perpetuity.

It is made available under a CC-BY-ND 4.0 International license .

To quantify the sensitivity of the solutions to deviations in the outcome of interest, we sampled solutions near the optimal solution using a Markov chain. This algorithm is initialized at the optimal solution identified by simulated annealing and the genetic algorithm and samples are drawn from a proposal distribution and accepted if they perform within the desired tolerance (0.25%) of the optimal solution.

B Results for additional scenarios

In this section we present detailed results for each alternative scenario. For simplicity we do not repeat extended figure captions, which follow those of main text Figures 2 and 3 (except for the stated scenario).

medRxiv preprint doi: https://doi.org/10.1101/2020.09.22.20199174; this version posted September 23, 2020. The copyright holder for this preprint (which was not certified by peer review) is the author/funder, who has granted medRxiv a license to display the preprint in perpetuity.

It is made available under a CC-BY-ND 4.0 International license .

B.1 Base model with age-only demographic groups (without essential workers)

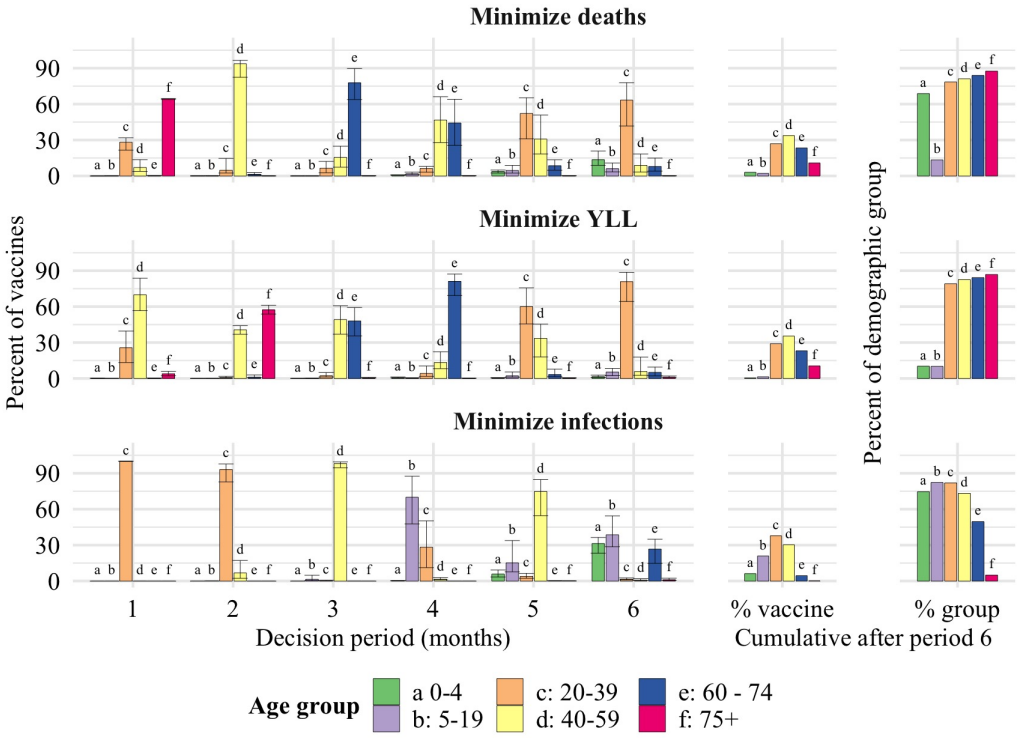

Figure 5: **Alternative scenario—Age-only groups:** The optimal allocation of vaccines between age groups at each decision time point. Each panel shows the solution for a given objective.

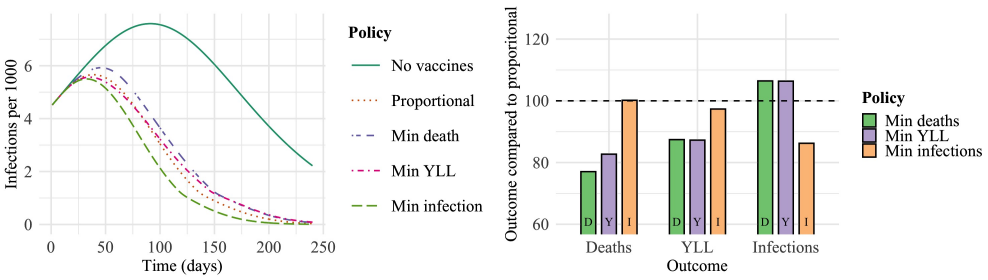

Figure 6: **Alternative scenario—Age-only groups:** The number of infections per 1,000 individuals over time under each policy (left) and the performance of each policy relative to a a uniform allocation policy (right).

medRxiv preprint doi: https://doi.org/10.1101/2020.09.22.20199174; this version posted September 23, 2020. The copyright holder for this preprint (which was not certified by peer review) is the author/funder, who has granted medRxiv a license to display the preprint in perpetuity.

It is made available under a CC-BY-ND 4.0 International license .

B.2 Strong NPI

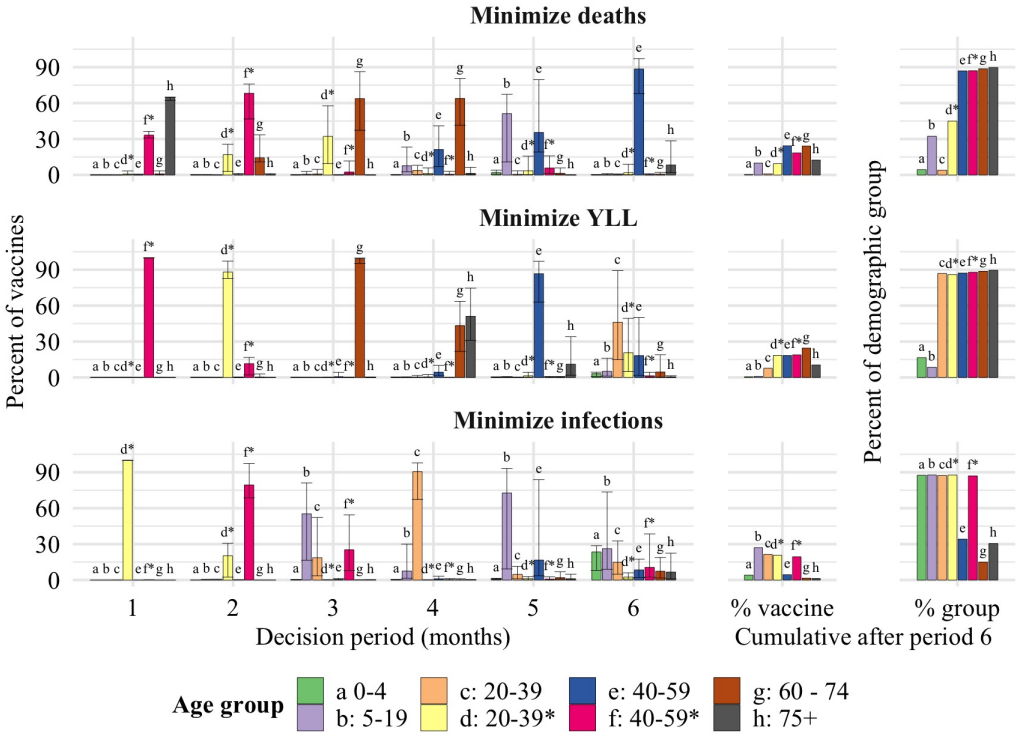

Figure 7: **Alternative scenario—Strong NPI:** The optimal allocation of vaccines between age groups at each decision time point. Each panel shows the solution for a given objective.

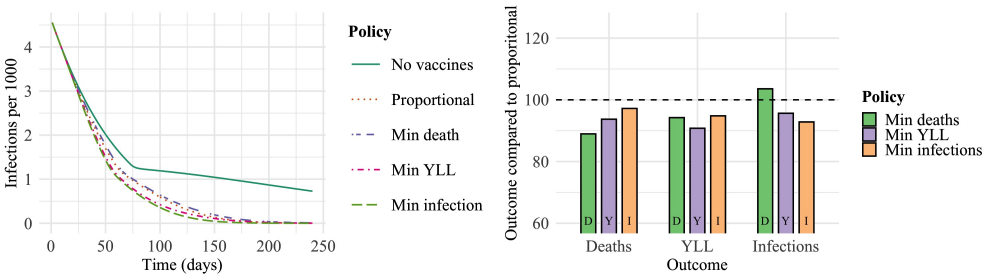

Figure 8: **Alternative scenario—Strong NPI:** The number of infections per 1,000 individuals over time under each policy (left) and the performance of each policy relative to a a uniform allocation policy (right).

medRxiv preprint doi: https://doi.org/10.1101/2020.09.22.20199174; this version posted September 23, 2020. The copyright holder for this preprint (which was not certified by peer review) is the author/funder, who has granted medRxiv a license to display the preprint in perpetuity.

It is made available under a CC-BY-ND 4.0 International license .

B.3 Weak NPI

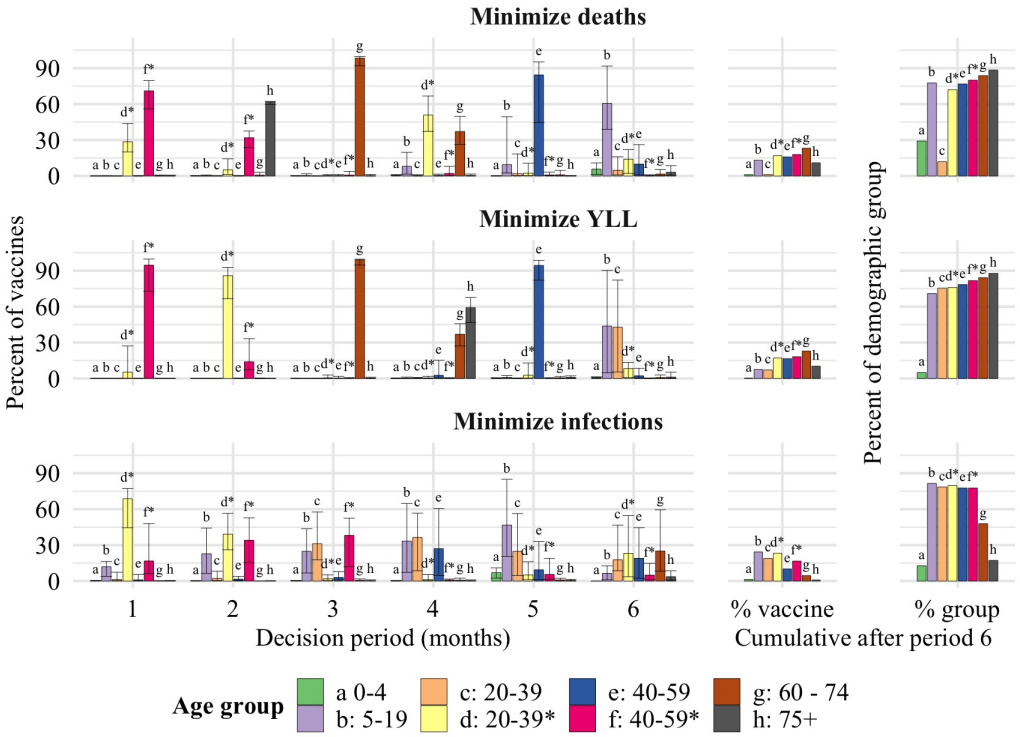

Figure 9: **Alternative scenario—Weak NPI:** The optimal allocation of vaccines between age groups at each decision time point. Each panel shows the solution for a given objective.

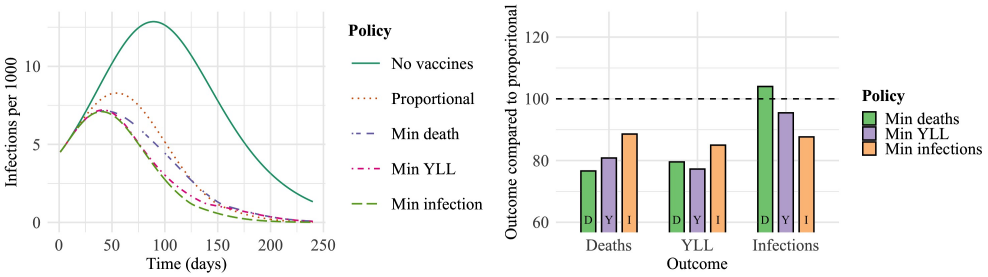

Figure 10: **Alternative scenario—Weak NPI:** The number of infections per 1,000 individuals over time under each policy (left) and the performance of each policy relative to a uniform allocation policy (right).

medRxiv preprint doi: https://doi.org/10.1101/2020.09.22.20199174; this version posted September 23, 2020. The copyright holder for this preprint (which was not certified by peer review) is the author/funder, who has granted medRxiv a license to display the preprint in perpetuity.

It is made available under a CC-BY-ND 4.0 International license .

B.4 Weak vaccine

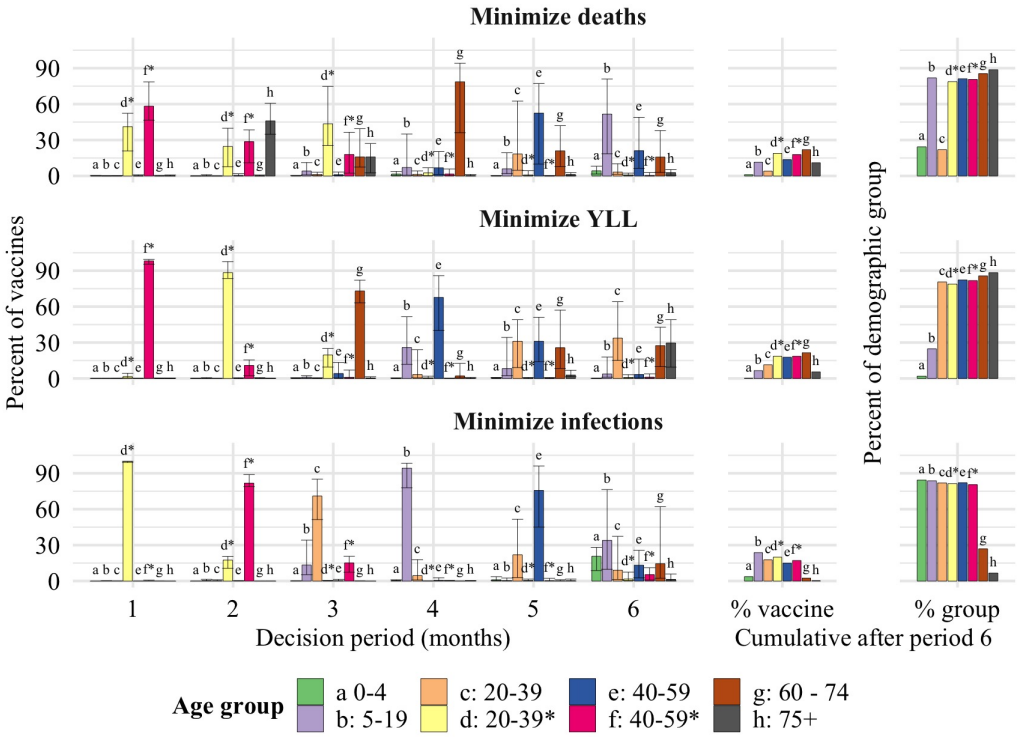

Figure 11: **Alternative scenario—Weak vaccine:** The optimal allocation of vaccines between age groups at each decision time point. Each panel shows the solution for a given objective.

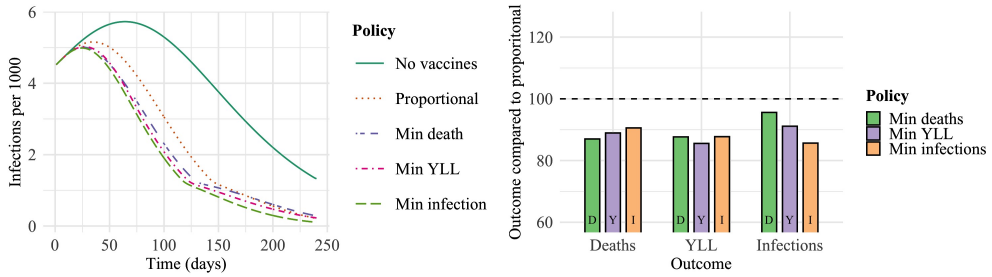

Figure 12: **Alternative scenario—Weak vaccine:** The number of infections per 1,000 individuals over time under each policy (left) and the performance of each policy relative to a uniform allocation policy (right).

medRxiv preprint doi: https://doi.org/10.1101/2020.09.22.20199174; this version posted September 23, 2020. The copyright holder for this preprint (which was not certified by peer review) is the author/funder, who has granted medRxiv a license to display the preprint in perpetuity.

It is made available under a CC-BY-ND 4.0 International license .

B.5 Weak vaccine in seniors

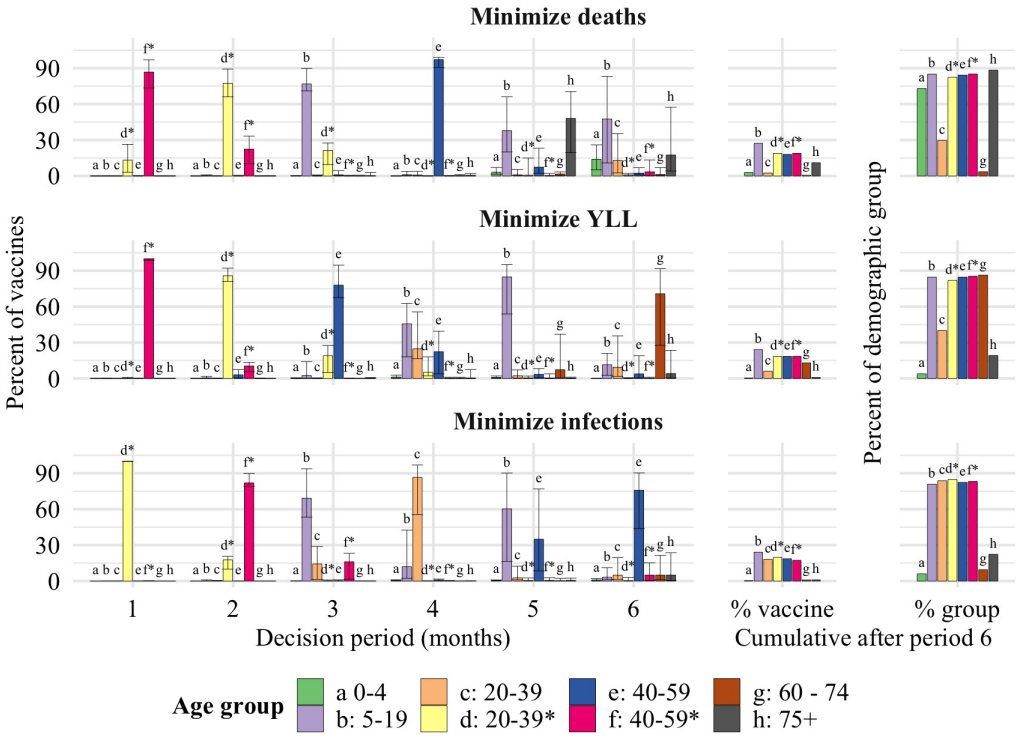

Figure 13: **Alternative scenario—Weak vaccine in seniors (ages 60+):** The optimal allocation of vaccines between age groups at each decision time point. Each panel shows the solution for a given objective.

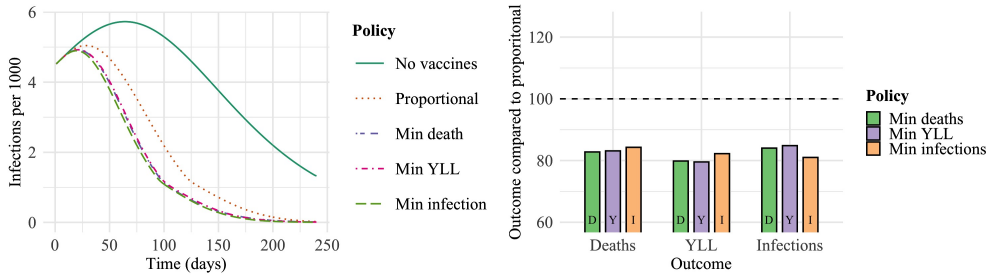

Figure 14: **Alternative scenario—Weak vaccine in seniors (ages 60+):** The number of infections per 1,000 individuals over time under each policy (left) and the performance of each policy relative to a uniform allocation policy (right).

medRxiv preprint doi: https://doi.org/10.1101/2020.09.22.20199174; this version posted September 23, 2020. The copyright holder for this preprint (which was not certified by peer review) is the author/funder, who has granted medRxiv a license to display the preprint in perpetuity.

It is made available under a CC-BY-ND 4.0 International license .

B.6 Lower child susceptibility

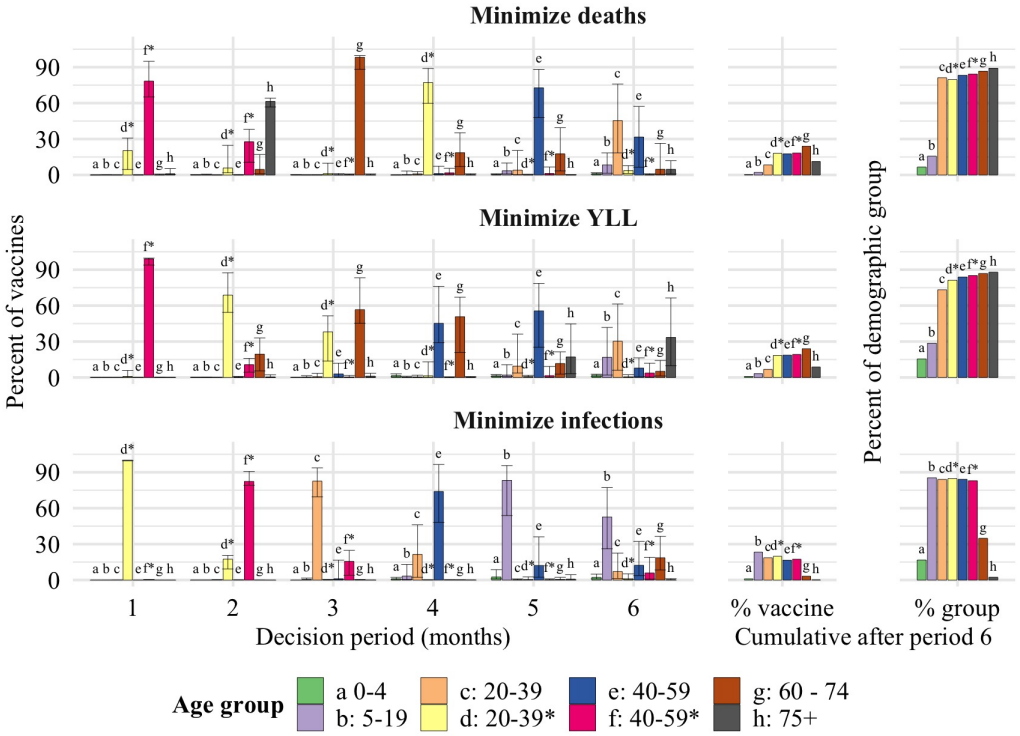

Figure 15: **Alternative scenario—lower child susceptibility (ages < 20):** The optimal allocation of vaccines between age groups at each decision time point. Each panel shows the solution for a given objective.

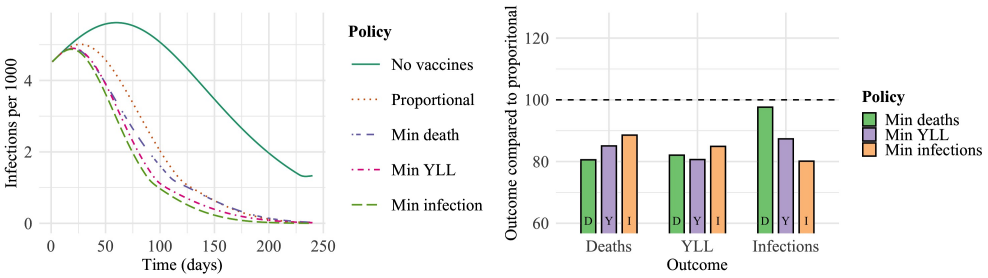

Figure 16: **Alternative scenario—lower child susceptibility (ages < 20):** The number of infections per 1,000 individuals over time under each policy (left) and the performance of each policy relative to a uniform allocation policy (right).

medRxiv preprint doi: https://doi.org/10.1101/2020.09.22.20199174; this version posted September 23, 2020. The copyright holder for this preprint (which was not certified by peer review) is the author/funder, who has granted medRxiv a license to display the preprint in perpetuity.

It is made available under a CC-BY-ND 4.0 International license .

B.7 Even susceptibility

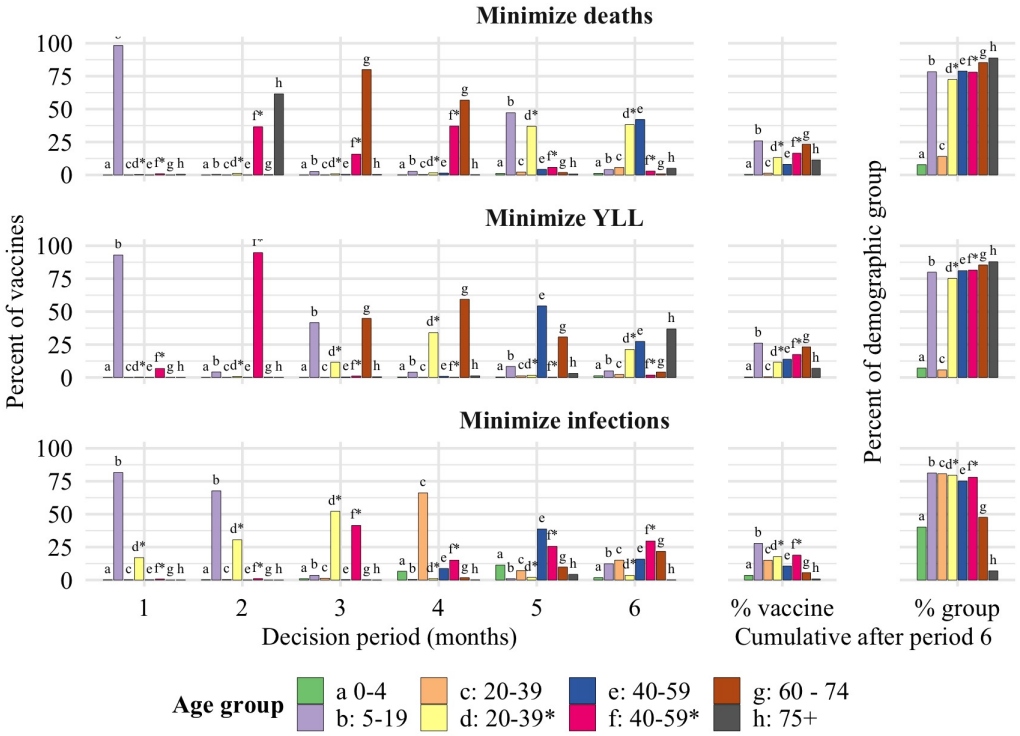

Figure 17: **Alternative scenario—Even susceptibility:** The optimal allocation of vaccines between age groups at each decision time point. Each panel shows the solution for a given objective.

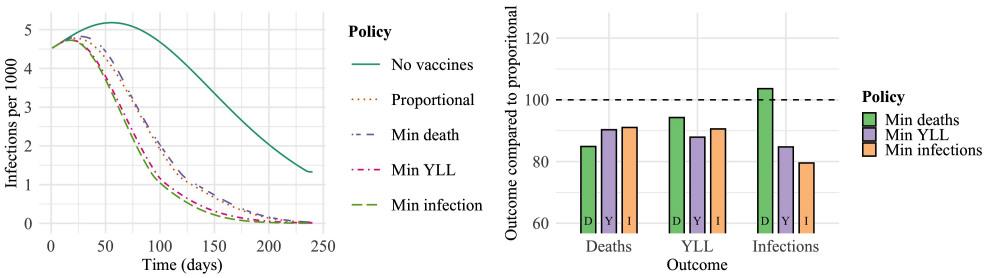

Figure 18: **Alternative scenario—Even susceptibility:** The number of infections per 1,000 individuals over time under each policy (left) and the performance of each policy relative to a uniform allocation policy (right).

medRxiv preprint doi: https://doi.org/10.1101/2020.09.22.20199174; this version posted September 23, 2020. The copyright holder for this preprint (which was not certified by peer review) is the author/funder, who has granted medRxiv a license to display the preprint in perpetuity.

It is made available under a CC-BY-ND 4.0 International license .

B.8 Ramp up

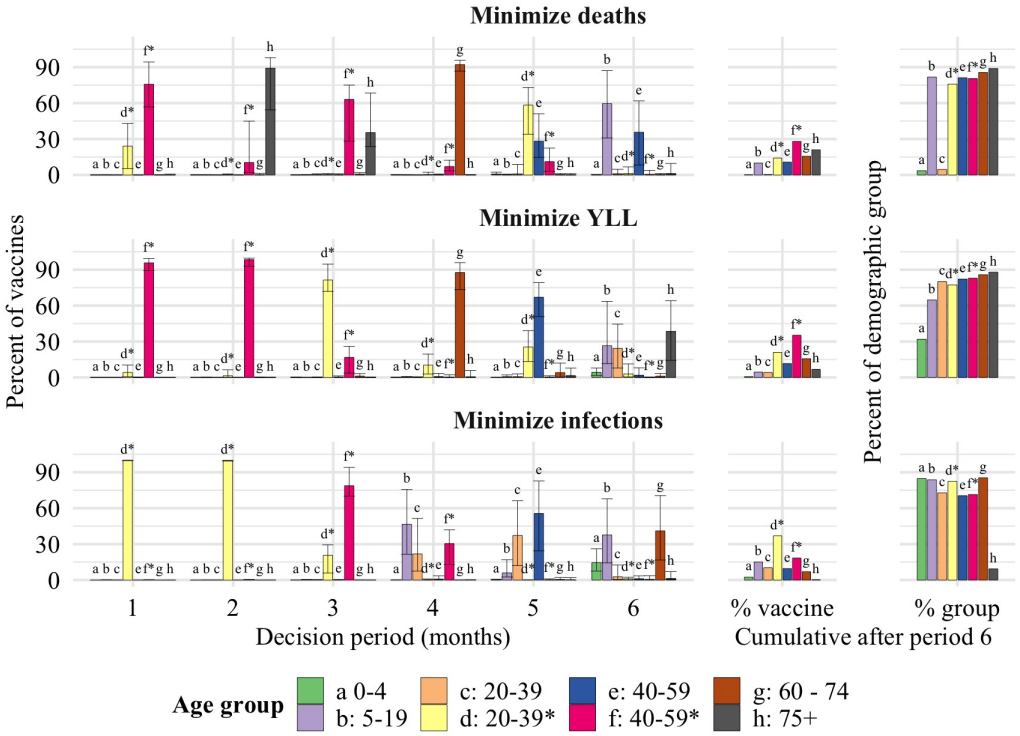

Figure 19: **Alternative scenario 4—Ramp up:** The optimal allocation of vaccines between age groups at each decision time point. Each panel shows the solution for a given objective.

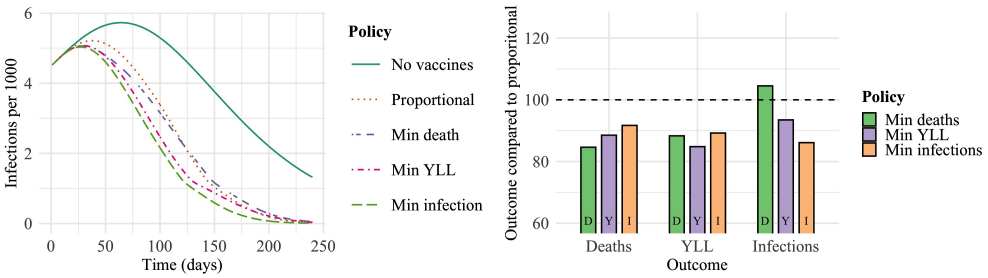

Figure 20: **Alternative scenario 4—Ramp up:** The number of infections per 1,000 individuals over time under each policy (left) and the performance of each policy relative to a a uniform allocation policy (right).

medRxiv preprint doi: https://doi.org/10.1101/2020.09.22.20199174; this version posted September 23, 2020. The copyright holder for this preprint (which was not certified by peer review) is the author/funder, who has granted medRxiv a license to display the preprint in perpetuity.

It is made available under a CC-BY-ND 4.0 International license .

B.9 Open schools

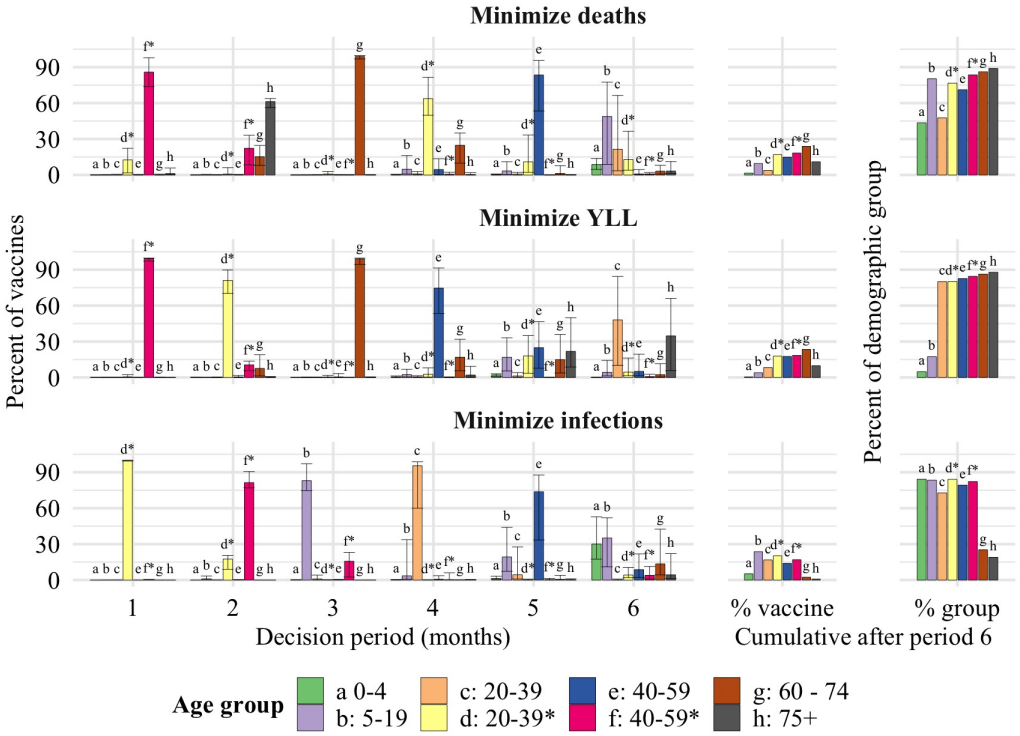

Figure 21: **Alternative scenario—Open schools:** The optimal allocation of vaccines between age groups at each decision time point. Each panel shows the solution for a given objective.

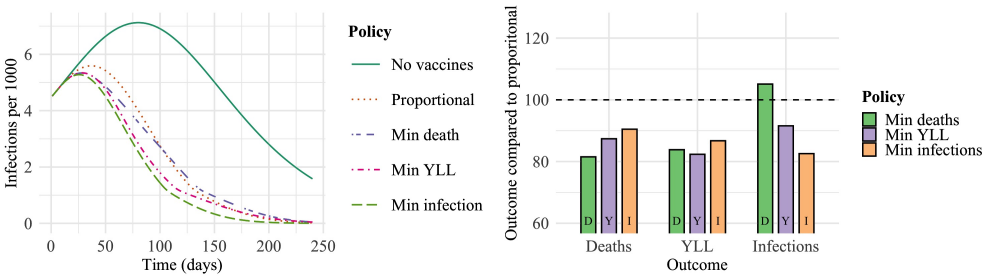

Figure 22: **Alternative scenario—Open schools:** The number of infections per 1,000 individuals over time under each policy (left) and the performance of each policy relative to a a uniform allocation policy (right).

medRxiv preprint doi: https://doi.org/10.1101/2020.09.22.20199174; this version posted September 23, 2020. The copyright holder for this preprint (which was not certified by peer review) is the author/funder, who has granted medRxiv a license to display the preprint in perpetuity.

It is made available under a CC-BY-ND 4.0 International license .

C Vaccine that is partially effective at the individual level

Vaccines can provide multiple form of protections against infections. Among these protections is the ability for vaccines to prevent individuals from becoming infected (the case considered in the main text). In addition, if vaccinated individuals still become infected they may (1) be less infectiousness and/or (2) develop less severe symptoms. To allow for these latter two cases we changed the model structure to track vaccinated and infected individuals. To do this we maintained the protected and uninfected category P and added four categories: vaccinated and exposed class P_{exp}, vaccinated and pre-symptomatic P_{presym}, vaccinated and asymptomatic P_{asym} and vaccinated and symptomatic P_{sym}. The three vaccine efficiencies are modeled by three age specific vectors, VE_{sucpt}, VE_{trans}, and VE_{sym}, which represent the amount the vaccine reduces the susceptibility of vaccinated individuals to infection, the reduction in infectiousness of vaccinated individuals and the reduction in infection fatality rate of vaccinated individuals. This new model can be described by the following system of equations:

$$\dot{S}_i = -qs_i\theta\left[\sum_{j\in J}\sum_{m\in M}\tau_m r_{m,i,j}S_i\frac{I_{m,j}}{N_j} + \tau_m r_{m,i,j}S_i\frac{P_{m,j}(1-VE_{trans})}{N_j}\right] - \mu_i v \tag{22}$$

$$\dot{P}_i = -qs_i(1-VE_{sucpt,i})\theta\left[\sum_{j\in J}\sum_{m\in M}\tau_m r_{m,i,j}P_i\frac{I_{m,j}}{N_j} + \tau_m r_{m,i,j}P_i\frac{P_{m,j}(1-VE_{trans})}{N_j}\right] + \mu_i v \tag{23}$$

$$\dot{E}_i = qs_i\theta\left[\sum_{j\in J}\sum_{m\in M}\tau_m r_{m,i,j}S_i\frac{I_{m,j}}{N_j} + \tau_m r_{m,i,j}S_i\frac{P_{m,j}(1-VE_{trans})}{N_j}\right] - E_i/D_{exp} \tag{24}$$

$$\dot{P_{exp,i}} = qs_i(1-VE_{sucpt,i})\theta\left[\sum_{j\in J}\sum_{m\in M}\tau_m r_{m,i,j}P_i\frac{I_{m,j}}{N_j} + \tau_m r_{m,i,j}P_i\frac{P_{m,j}(1-VE_{trans})}{N_j}\right] - E_i/D_{exp} \tag{25}$$

$$\dot{I}_{pre,i} = E_i/D_{exp} - I_{pre,i}/D_{pre} \tag{26}$$

$$\dot{P}_{pre,i} = P_{exp_i}/D_{exp} - P_{pre,i}/D_{pre} \tag{27}$$

$$\dot{I}_{asym,i} = \sigma_{asym}I_{pre,i}/D_{pre} - I_{asym,i}/D_{asym} \tag{28}$$

$$\dot{P}_{asym,i} = \sigma_{asym}P_{pre,i}/D_{pre} - P_{asym,i}/D_{asym} \tag{29}$$

$$\dot{I}_{sym,i} = (1-\sigma_{asym})I_{pre,i}/D_{pre} - I_{sym,i}/D_{sym} \tag{30}$$

$$\dot{P}_{sym,i} = (1-\sigma_{asym})P_{pre,i}/D_{pre} - P_{sym,i}/D_{sym} \tag{31}$$

$$\dot{R}_i = I_{asym,i}/D_{asym} + (1-\delta_i)I_{sym,i}/D_{sym} + (1-\delta_i\,(1-VE_{sym}))P_{sym,i}/D_{sym} \tag{32}$$

$$\dot{D}_i = \delta_i(1-VE_{sym})P_{sym,i}/D_{sym} + \delta_i(1-VE_{sym})I_{sym,i}/D_{sym} \tag{33}$$

We consider three cases. For comparison with the Base model, we consider the same level of efficacy: $VE_{sym} = VE_{sucpt} = VE_{trans} = 65\%$. Next we consider a vaccine that is more effective at reducing the severity of illness but less effective at preventing infection and transmission. We consider a moderate case where $VE_{sym} = 70\%$ and $VE_{sucpt} = VE_{trans} = 30\%$. Finally we consider a more extreme case where $VE_{sym} = 90\%$ and $VE_{sucpt} = VE_{trans} = 10\%$. These three scenarios will be referred to as the "All 65%", "70%-30%", and "90%-10%" scenarios, respectively.

Iterations of main text Fig. 2 and Fig. 3 for these three alternative scenarios are shown further below. To compare and contrast cumulative vaccination results, directly below in Fig. 23 we show for the Base model and the three alternative scenarios the percentage of each group vaccinated after three months (left panel) and six months (right panel). In general, results are similar between the Base model with 65% of individuals 100% protected when vaccinated and the alternative where vaccines are 65% effective for all vaccinated. When shifts are apparent at either three or six months, they typically involve younger essential workers or younger seniors.

Over all scenarios, we find that results after three months are sensitive in specific cases. When minimizing deaths or infections, results are relatively insensitive. A notable exception is for infections under the extreme scenario (90%-10%), we see a shift away from school age children to the youngest and oldest. When minimizing YLL, we found substantial shifts between three groups: younger essential workers, younger seniors and older seniors.

After six months, the sensitivity and shifting lies mostly with younger groups (under 40) when focused on mortality (deaths or YLL) and conversely with older groups (over 40) when focused on infections (except for the extreme case, 90%-10%).

medRxiv preprint doi: https://doi.org/10.1101/2020.09.22.20199174; this version posted September 23, 2020. The copyright holder for this preprint **(which was not certified by peer review)** is the author/funder, who has granted medRxiv a license to display the preprint in perpetuity.

It is made available under a CC-BY-ND 4.0 International license .

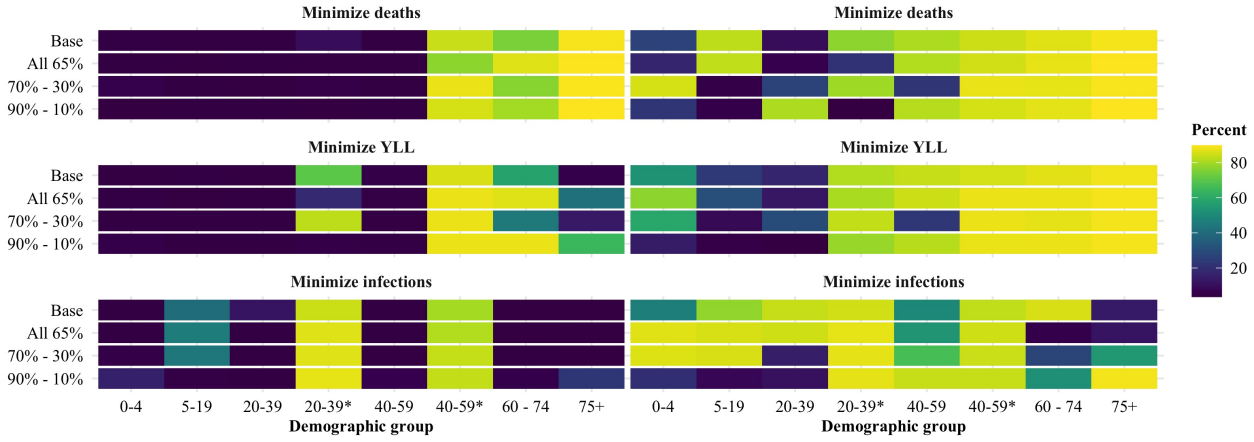

(a) Three months

(b) Six months

Figure 23: The cumulative percent of each demographic group (x-axis) vaccinated after three or six months under the Base model and three alternative scenarios for partial vaccine efficacy (y-axis) for each objective (panel). Vaccine supply is sufficient to vaccinate 10% of the population each month.

medRxiv preprint doi: https://doi.org/10.1101/2020.09.22.20199174; this version posted September 23, 2020. The copyright holder for this preprint (which was not certified by peer review) is the author/funder, who has granted medRxiv a license to display the preprint in perpetuity.

It is made available under a CC-BY-ND 4.0 International license .

C.1 Vaccine reducing mortality and spread equally

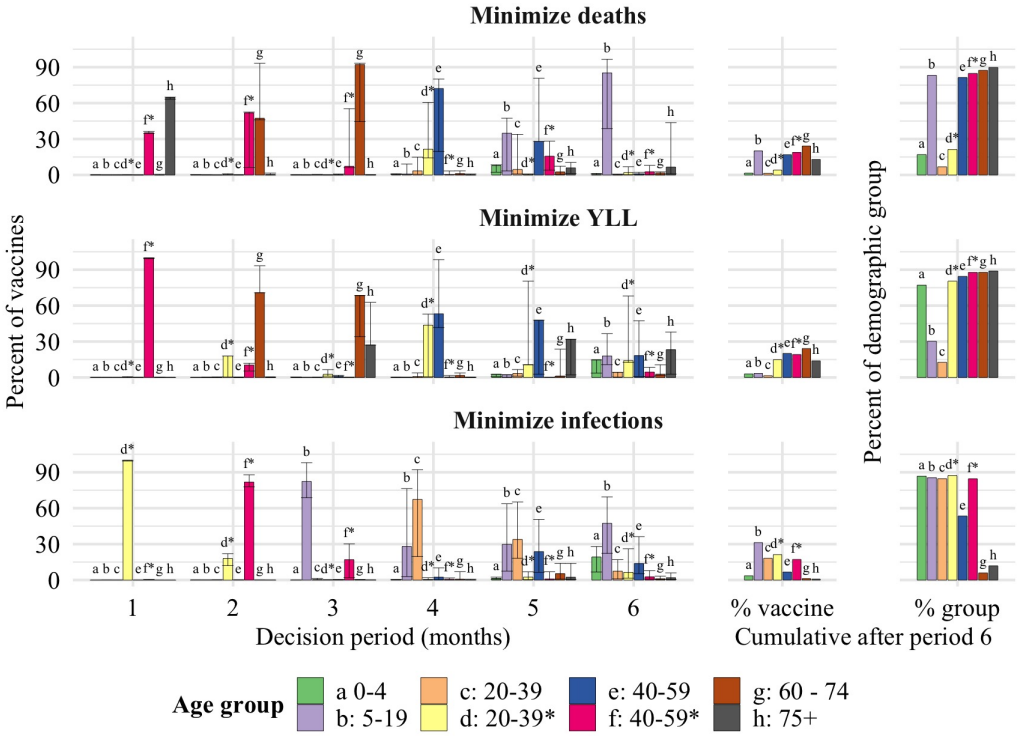

Figure 24: **Alternative scenario—Partially effective vaccine, reduces susceptibility, transmission and infection fatality rate by 65%.**

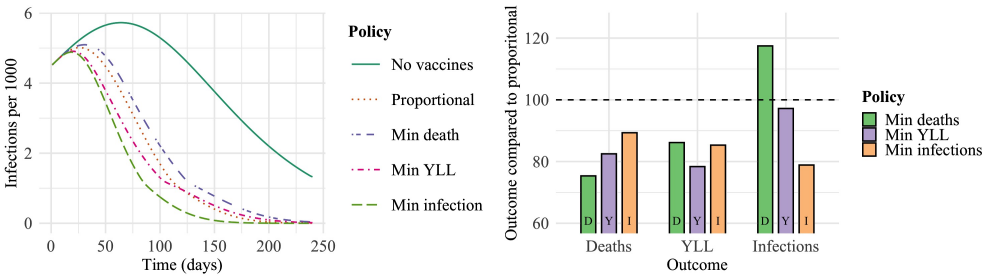

Figure 25: **Alternative scenario—Partially effective vaccine, reduces susceptibility, transmission and infection fatality rate by 65%.**

medRxiv preprint doi: https://doi.org/10.1101/2020.09.22.20199174; this version posted September 23, 2020. The copyright holder for this preprint (which was not certified by peer review) is the author/funder, who has granted medRxiv a license to display the preprint in perpetuity.

It is made available under a CC-BY-ND 4.0 International license .

C.2 Vaccine reducing mortality more than spread (moderately)

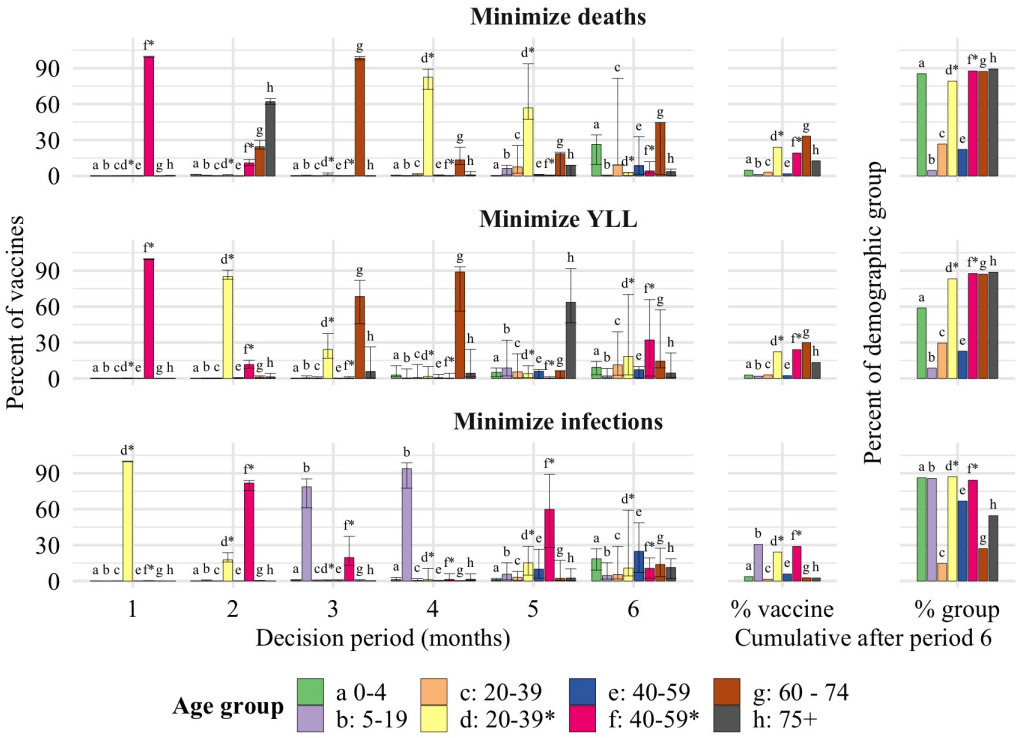

Figure 26: **Alternative scenario—Vaccine reducing mortality more than spread (moderately).**

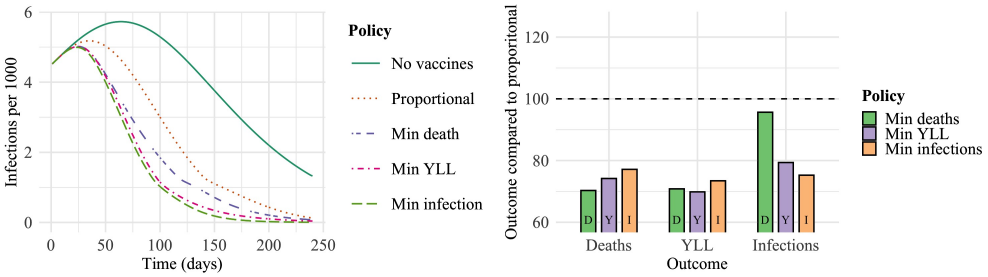

Figure 27: **Alternative scenario—Vaccine reducing mortality more than spread (moderately).**

medRxiv preprint doi: https://doi.org/10.1101/2020.09.22.20199174; this version posted September 23, 2020. The copyright holder for this preprint (which was not certified by peer review) is the author/funder, who has granted medRxiv a license to display the preprint in perpetuity.

It is made available under a CC-BY-ND 4.0 International license .

C.3 Vaccine reducing mortality more than spread (strongly)

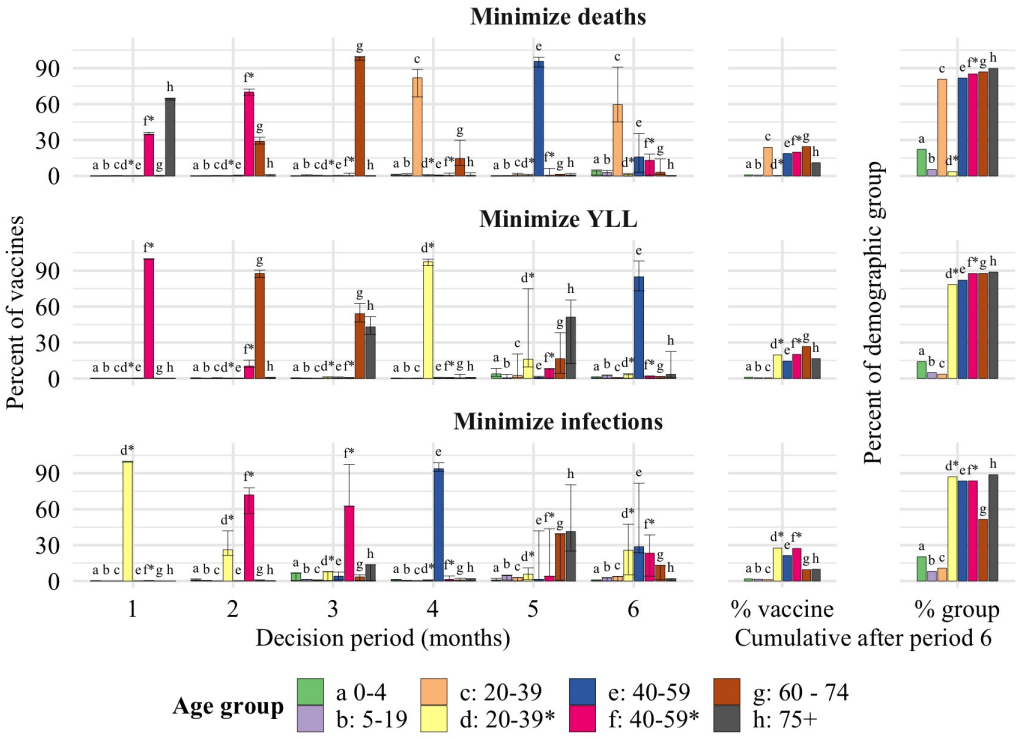

Figure 28: **Alternative scenario—Vaccine reducing mortality more than spread (strongly).**

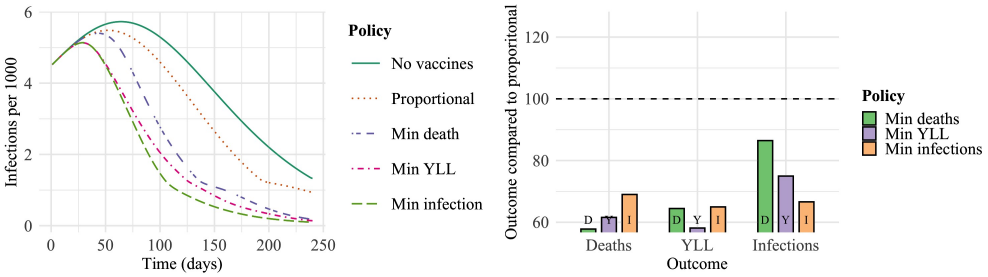

Figure 29: **Alternative scenario—Vaccine reducing mortality more than spread (strongly).**